# A Comparison Between Novel FPGA-Based Pad Monitoring System Using Ballistocardiography and the Conventional Systems for Synchronization and Gating of CMRI at 3 Tesla: A Pilot Study

**RADEK MARTINEK** [1], **JINDRICH BRABLIK** [1], **JAKUB KOLARIK** [1], **MARTINA LADROVA** [1], **JAN NEDOMA** [2], **RADANA KAHANKOVA** [1], **RENE JAROS** [1], **LUBOMIR VOJTISEK** [3], **AND PAVLA HANZLIKOVA** [4]

[1]Department of Cybernetics and Biomedical Engineering, Faculty of Electrical Engineering and Computer Science, VŠB–Technical University of Ostrava, 708 00 Ostrava, Czech Republic
[2]Department of Telecommunications, Faculty of Electrical Engineering and Computer Science, VŠB–Technical University of Ostrava, 708 00 Ostrava, Czech Republic
[3]Central European Institute of Technology (CEITEC), Masaryk University, 601 77 Brno, Czech Republic
[4]Department of Imaging Method, Faculty of Medicine, University of Ostrava, 703 00 Ostrava, Czech Republic

Corresponding author: Radek Martinek (radek.martinek@vsb.cz)

**ABSTRACT** This pilot pre-clinical study demonstrates the applicability of a new type of pneumatic cardiac triggering (PCT) for cardiac imaging. The pilot research compares the novel FPGA-based pad monitoring system for cardiac triggering using ballistocardiography (BCG) with conventional systems based on electrocardiography (ECG) and photoplethysmography (PPG). The implemented system enables cardiac triggering without the need to fix the sensors to the patient's body. This unique approach has the potential to reduce the preparation time for examination and the examination itself and to increase patient's comfort. The pilot pre-clinical study was conducted on 10 subjects at the Siemens Prisma 3T MRI Scanner within the CEITEC Multimodal and Functional Imaging Laboratory - Central European Institute of Technology, Masaryk University, upon the approval of the Ethics Committee. In total, 748 peaks (heart beats) were detected, with 7.347 correctly identified as true positive peaks, 140 incorrectly detected as false positive peaks, and 106 missed peaks (false negative). For all subjects, the total accuracy reached 96.31% and F1 score reached 98.18%. The applicability of the proposed BCG system was also analyzed in terms of objective (BRISQUE, NIQE, PIQE) and subjective evaluation of the images by 10 experts. The study compares images from two basic cardiac sequences - TRUE FISP (Free Induction Decay Steady-State Precession) and PSIR (Phase Sensitive Inversion Recovery) sequences. The BCG system achieves comparable results with the most frequently used and most accurate clinical ECG system used as gold standard. The results prove that the BCG signal captured by our new sensor can be used as a substitute for ECG signal during MRI exam with reliability of 97%.

**INDEX TERMS** Cardiac triggering, triggering using ballistocardiography (BCG), pad monitoring system, imaging of the heart, electrocardiography (ECG), photoplethysmography (PPG), cardiac magnetic resonance imaging (CMRI).

The associate editor coordinating the review of this manuscript and approving it for publication was Mauro Fadda.

## I. INTRODUCTION
Magnetic resonance (MR) imaging is increasingly important in the process of examination of human body structures.
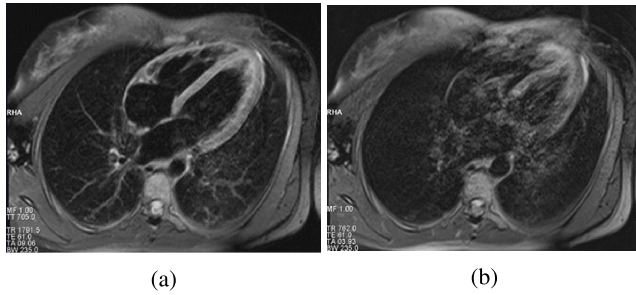
**FIGURE 1.** An example of the effect of CMRI synchronization with the cardiac activity (T2w fat suppression sequence): (a) - CMRI with triggering, (b) - CMRI without triggering.



**FIGURE 2.** The waveform of the ECG signal measured: (a) outside the MR environment, (b) within the MR environment with an intensity of 1.5 T, where both the R wave and the T wave acquire similar amplitudes.

Cardiac magnetic resonance imaging (CMRI) is used for a specific area of heart structure and function imaging. This type of examination is important both in the diagnosis of inflammatory and ischemic diseases, as well as in the detection of myocardial injury and myocardial fibrosis allowing better treatment and prevention or delay the progression of the disease [1]. Because the heart is always in motion, triggering synchronization is used in clinical practice to ensure a high-quality image. This technique provides high temporal and spatial resolution of the image by monitoring cardiac or respiratory activity, according to which MR acquisition is triggered. The aim is to trigger an acquisition with minimal movement of the heart (i.e. the terminal phase of the diastole or systole), which causes numerous movement artifacts, manifesting themselves as shadows and blurred contours in the image [2], see Fig. 1.

The principle of triggering is to detect the most prominent point of the signal that indicates the cardiac systole. In current clinical practice, cardiac activity is monitored by electrocardiography (ECG), which is, in some cases, replaced by a peripheral pulse signal (i.e. PPG). The course of these measurements and their advantages and disadvantages are described below.

Electrocardiography, one of the best known and most widespread methods of cardiac activity monitoring, is measured by several electrodes located on the patient's chest, wherein the number and placement of the electrodes vary according to the information to be received by the scan. Three or four electrodes are standardly used to record R peaks in CMRI triggering [3]. Although ECG is a means for quick and accurate recording of cardiac function, when measuring in an MR device environment, numerous problems arise, such as magnetic field artifacts [4] or even electrode heating due to high voltage induction in the ECG hardware, resulting from the interaction of the ECG system with the radiofrequency and gradient systems [5], [6]. To avoid unwanted currents in the ECG leads due to the rapid switching of gradient fields, the leads must be located in such a way that no loops are present, and the wires should be as short as possible. Furthermore, the conductors are located outside the resonators to suppress the interaction with the RF field [7].

When measuring ECG in the magnetic field of an MR device, the so-called magnetohydrodynamic (MHD) effect,
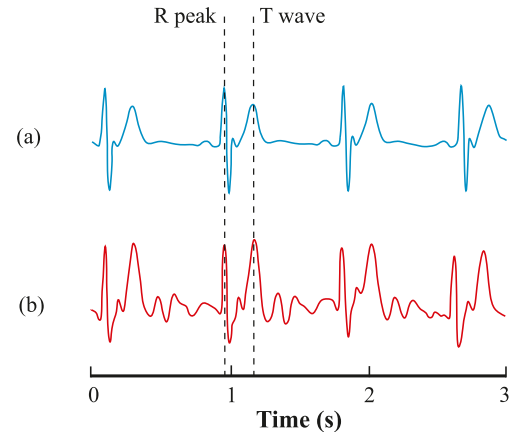
which is caused by the movement of blood that is electrically conductive and the consequent generation of an added electric current, is a very undesirable problem. This artifact causes ECG signal distortion by affecting the T wave (see Fig. 2), thus preventing proper detection of the R wave and the subsequent synchronization [7]. The issue of MHD artifact grows with the increasing intensity of the magnetic field. The higher intensity of the magnetic field promises an increase of contrast in the image and noise suppression. For example, Krug *et al.* [8] and Snyder *et al.* [9] have shown that triggering with ECG signal is unsuitable for intensities higher than 3T. Frauenrath *et al.* [10] report that the error rate while determining the ECG heart rate is up to 30%. According to [11], the amplitude of the T wave may exceed the R wave by 20% of its amplitude (i.e. an increase in the amplitude by about 315% of the original T wave), already at a field strength value of 1.5 T. Due to the susceptibility of the ECG to the influence of the MHD effect, new methods of detecting R waves and suppression of this artifact are currently being developed, [12] and [13], and, also, new ways of sensing cardiac activity are being sought.

In addition to the aforementioned pitfalls of ECG measurements in the MR environment, the ECG examination itself is inconvenient for the patient as it is necessary to prepare the skin well at the locations of the ECG electrodes to ensure optimal contact of the electrode with the skin. To eliminate the noise being produced due to poor contact, hair must be shaved immediately before the examination and the skin surface must be scrubbed with a mild abrasive soap (gel) [14].

The PPG triggering is a suitable alternative to triggering using the ECG signal. The measurement is considerably simpler than in the case of ECG, where the sensor is most often placed on the finger of the hand, and also resistant to artifacts arising due to the influence of the magnetic fields [15]. The PPG signal is measured by a light sensor operating on the principle of sensing changes in light absorption by blood, which corresponds to the change in its volume. The rise and fall of the wave thus reflects the process of cardiac
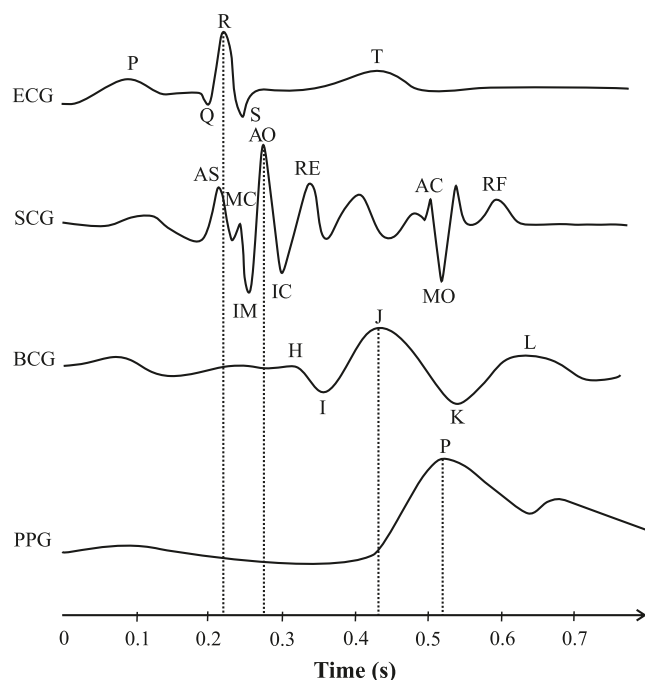
**FIGURE 3.** Physiological delay between signals used for MR triggering with triggering pulses marked.

systole and diastole. However, PPG measurement for CMRI triggering is not standardly used because the delay between the cardiac activity and the output signal caused by the transit time of blood from the heart to the peripheral scan site is striking. This delay can be in the order of several hundred milliseconds and depends on the patient's (patho)physiology (see Fig. 3) [10].

Due to the numerous pitfalls of these established triggering methods, new techniques and sensors for sensing cardiac activity for the purpose of CMRI acquisition triggering that are resistant to artifacts arising during measurements in the MR environment are being sought and developed. One of these methods is the so-called self-gating technique, [16]–[19], which is already in use in clinical practice. The self-gating method uses information on organ movement directly from the MR signals by monitoring the changes in the total transverse magnetization. The advantage of this technique is the absence of additional hardware placed on the patient's body. However, these techniques fall behind in cases of tachycardia and cases where myocardial contraction and relaxation are very mild throughout the cardiac cycle [16], [20]. Other methods of research are, for example, ultrasonic methods, [21]–[24], which promise resistance to MR environment artifacts, however, placing the ultrasonic probe on the patient's body lags behind other methods in simplicity. Optical fibres and sensors, which can also be used for MR environment measurement, are a modern approach to measuring medical signals, [25]–[31], due to their very weak interaction with its magnetic and other effects on the optical signal, and they promise a relatively inexpensive and simple alternative to CMRI triggering.

The use of an acoustic sensor, whose efficiency has been demonstrated both on instruments of magnetic intensity up to 3T and ultra-high magnetic field intensity of 7T, already achieves significant results, [10], [20], [32]–[35]. According to [33], an error of less than 1% is achieved during triggering by the acoustic signal as well as during magnetic field intensity of 7T, since the cardiac activity acoustic signal is immune to artifacts resulting from the magnetic field of the MR device. In comparison to conventional ECG measurements, this method has the advantage of simplifying patient preparation, reducing the number of cables and sensors, or avoiding the induction of high voltages that could hurt the patient [20], [32]. The disadvantage of the acoustic signal is the sensitivity to noise arising from the switching of gradient coils. The acoustic noise must then be filtered out of the signal [10] or the acoustic signal is converted to an optical signal and is fed through the optical fibre, thus avoiding any interaction of the scanning device with a static magnetic, gradient or RF field [32]. When compared to the ECG signal, another disadvantage may be the delay; Becker *et al.* [20], however, state that a delay of about 30 ms occurring between the first heart sound and the detected ECG R wave has no effect on CMR imaging by retrospective triggering.

Figure 3 shows the physiologic delay between the ECG and other signals that the study addresses (SCG, BCG, and PPG). The delay length depends on the patient's (patho)physiology as well as the design of the sensor itself. However, the total delay of the triggering signal (indicated by dotted lines) can be much longer due to the propagation of the signal by the medium to the control unit, the influence of filtering or the electronics controlling the state, and conversion of the signal [35], [36]. Such a delayed triggering signal then results in image acquisition in the wrong phase of the cardiac cycle, which leads to a reduced likelihood of proper diagnosis and often to the need for repeating the image acquisition, thereby extending the examination time.

The authors of the study have already developed a hybrid acoustic sensor for triggering MR acquisition based on seismocardiography (SCG) [36], which refers to monitoring of human body surface vibrations due to cardiac wall movement commonly sensed by accelerometers. In the past, the SCG signal was used to detect heart rate [37] and also to measure cardiac activity in the MR environment [38]. Although this sensor achieved very satisfactory results with part of the subjects measured, there were often problems with placing the sensor itself on the patient's body, which led to a deterioration in the quality of detection of significant features (A0-A0) and thus to worse CMRI synchronization.

This phenomenon inspired the authors to an idea to design a new type of pneumatic sensor without the need for fixing it on the patient's body; the patient would only be placed on this sensor, which would not have to be fixed in any way. The system is framed as FPGA-based pad monitoring. It is the use of field programmable gate array (FPGA) technology that minimizes the signal delay due to its processing (filtering, detection, etc.). This study evaluates the measurement

results with this new approach to measuring cardiac activity and the quality of the resulting MR images triggered by the BCG signal compared to conventional ECG and PPG signal measurement approaches.

## II. METHODS

The new type of sensor works on the principle of ballistocardiography (BCG). There are a number of studies [28], [39], [40] using the BCG principle. The substantial difference between BCG and SCG signal sensing [41]–[43] consists in the source of mechanical vibrations. In the case of the SCG signal, heart movement is the source of mechanical vibrations and, with BCG, it is the movement of blood through the bloodstream. The design of the sensor thus had to meet the requirement for the highest possible contact area between the sensor and the patient's soft tissues. Due to the patients lying position on their back with their legs stretched straight along the body, several potentially attractive sensor placement locations come to existence. The sensor design represents a distributed measuring system, which minimizes the delay between the ECG and BCG signals. Standard BCG sensing is usually performed by sensing the forces exerted on the bed by the patient's entire body. This is usually done by placing strain gauges at the point of contact of the bed with the floor. However, BCG signal acquisition can also be conducted locally, near major arteries, for example in the armpit or in the buttocks area. To ensure the best possible signal gain when sensing the BCG signal, the sensor has been designed in such a way that its contact area reaches the greatest possible contact with the patient's soft tissue.

### A. SENSOR EMBODIMENT

The sensor consists of a closed pneumatic system with a deformable sensor consisting of a tube or bellows of a non-metallic and airtight material, a transmission line and a measuring apparatus located outside the MR field. Preferably, materials such as polyvinyl chloride (PVC), polyurethane (PUR) or silicone are used to construct the sensor and the transmission line. The primary sensor version consists of a bed with a pacient circuit along the entire length of the patient's body and a reference circuit outside the patient's body, see Fig. 4. The reference sensor is used for post-processing of the signal and adaptive noise cancellation [44]–[46]. The sensor also exists in other embodiments, which can be placed locally under the patient's body or close to the arteries, in the form of a measuring spiral or bellows. In this local embodiment, the signal measured is SCG, not BCG as in this study.

When studying monitoring of cardiorespiratory activity in magnetic resonance, the sensor version in the bed-tube embodiment was primarily used. The bed consists of two parts, namely the sensing part and the insulating part. The sensing part includes a measuring tube and padding in order to enhance the patient's comfort. The insulating part then reduces the vibrations transmitted by the magnetic resonance structure. The sensor in the bed embodiment, as well as its
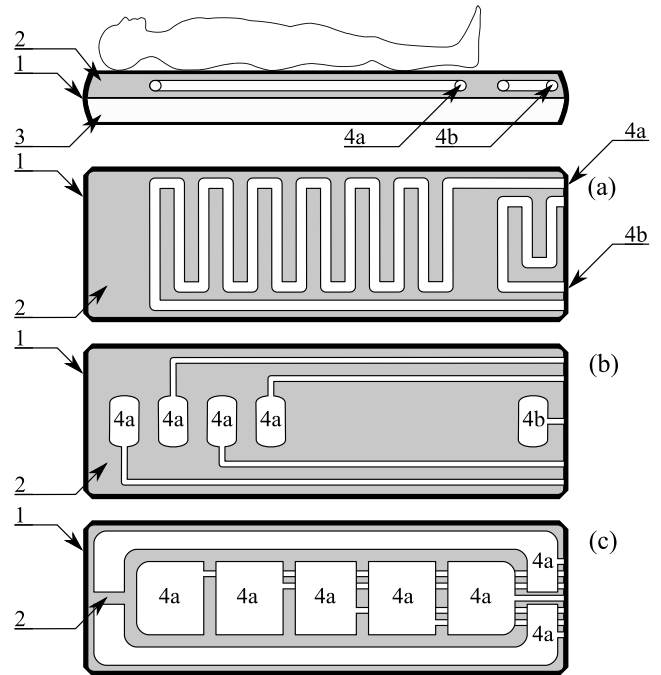


**FIGURE 4.** BCG sensor for monitoring cardiorespiratory activity; (a) tubular embodiment, (b) chamber embodiment (bellows), (c) chamber embodiment for monitoring the patient on the bed, where (1) bed case, (2) measuring part, (3) acoustic insulation, (4a) pacient circuit, (4b) reference circuit.

other versions, is equipped with connectors for linking to the transmission line, which conducts the signal out of the room where the magnetic resonance is located.

The sensor works on the principle of sensing movements of the patient's body as a result of the cardiorespiratory activity. These movements deform the sensor, thus modulating the pressure of the gaseous medium enclosed therein. The transmission line connects the sensor itself and the measuring apparatus, thereby forming a closed pneumatic system, see Fig. 5. Due to the construction material of the sensor and the transmission line consisting of non-metallic materials, neither the MRI function nor the sensor is affected. By using the pneumatic transmission line between the magnetic resonance room and the control room, the information on the patient's cardiorespiratory activity is transmitted. This information is transmitted as a function of tube pressure and reaches a speed nearing the speed of sound. In addition to the delay of the BCG signal in comparison with the reference ECG signal, it is also necessary to take into account the delay in transmission caused the propagation of the pressure change through the tube. The issue of delays between the ECG and the BCG, or the SCG, is discussed in detail in study [36]. In general, any pressure sensor can be used to measure the pressure inside the pneumatic system. Since the pressure in the tube corresponds approximately to atmospheric pressure, and only small changes occur, a microphone was used for the prototype of this sensor.

Figure 6a shows the sensor version implemented in the bed embodiment (BCG) with a tube within the pilot pre-clinical
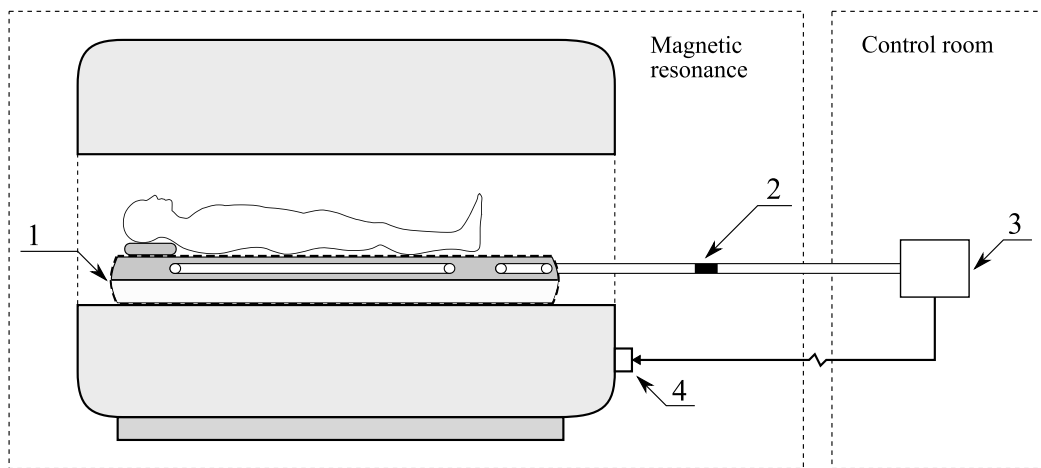
**FIGURE 5.** Installation of the BCG sensor in a magnetic resonance chamber - the bed embodimen: (1) sensor in the bed embodiment, (2) connector for linking to the transmission line, (3) measuring system, (4) magnetic resonance imaging switching.
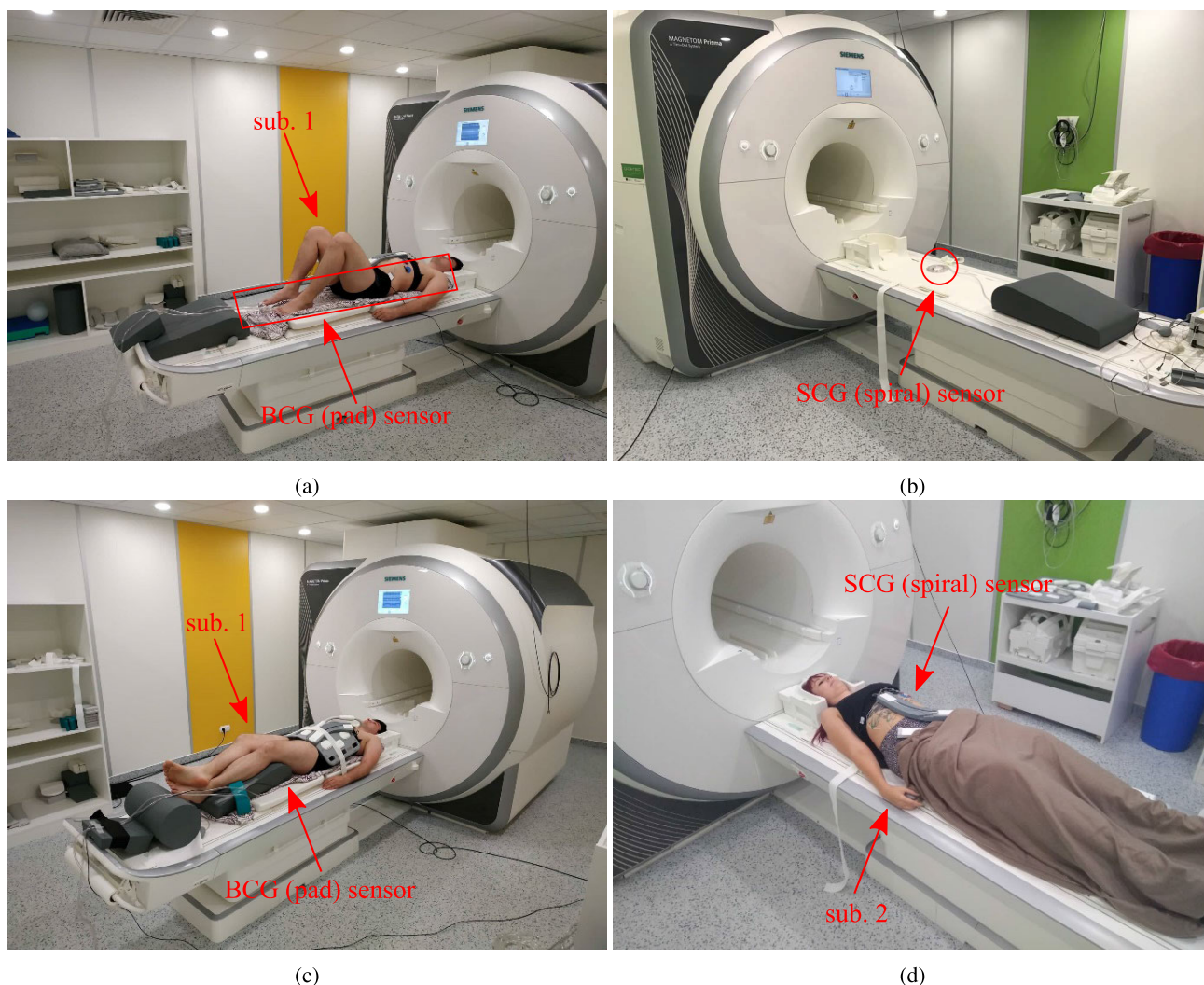


(a)

(b)

(c)

(d)

**FIGURE 6.** Installation of the BCG sensor in the pad (a, c) and the SCG spiral sensor (b, d) on the Siemens Prisma 3T MR scanner.

study carried out on a Siemens Prisma 3T MR scanner. Figure 6b shows the spiral-shaped (SCG) sensor. Figure 6c

shows a patient prepared for examination by the sensor located in the bed embodiment with a tube within the pilot
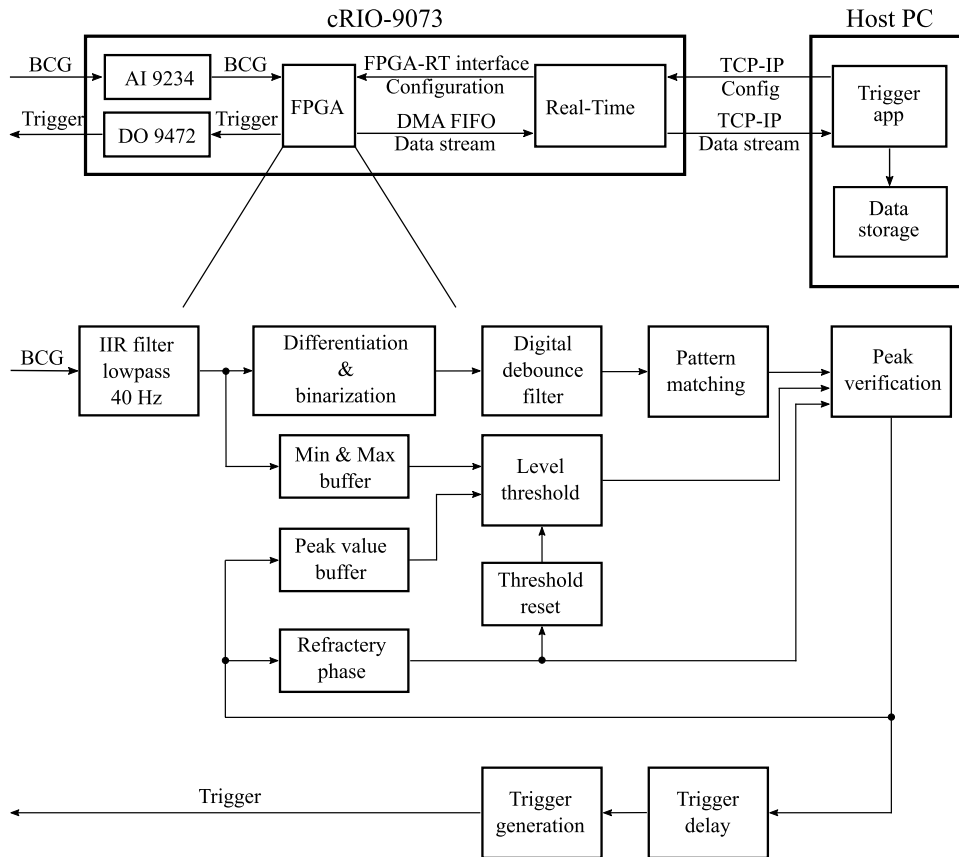
**FIGURE 7.** A detailed block diagram of the triggering system.

pre-clinical study. In Fig. 6d, the patient is prepared for measurement using a spiral-shaped sensor located below the left shoulder blade.

### B. DESCRIPTION OF THE MEASURING SW AND HW

The measuring and triggering systems are based on the concepts of virtual instrumentation. The main component of the system is a compact Reconfigurable Input Output (cRIO) controller comprised of a FPGA, a Real-Time operating system (RTOS) and a chassis that allows input/output modules to be connected to the cRIO system. Microphone and analogue input modules were used to measure the BCG signal; a digital output module was used to generate a triggering signal for magnetic resonance sequences. The second part of the measuring and triggering system is a laptop with a LabVIEW application that serves as the user interface. The application displays the BCG waveform measured, the peaks detected and the triggers generated in real-time and allows the user to configure the peak detection algorithm and the triggering delay defined. The hardware and software setup utilized was identical with the ones used in our previous research [36]. A complete block diagram of the system with the detailed description of the peak detection and the trigger generation logic implemented in FPGA is shown in Fig. 7.

The peak detection algorithm was adjusted to make it less dependent on the user configuration. The first improvement is represented by the "Min & Max buffer" block, which stores positive and negative extremes detected in the previous several seconds of the signal and uses them to define the initial threshold level for peak detection in case of reset (either user generated or internal). The initial threshold level was manually defined by the user in the previous version. The second improvement, newly represented by the "threshold reset block", generates internal reset of the peak detection algorithm in case that no peak is detected within a multiple of time defined by the refractory period (i.e. the phase after peak detection when the subsequent peak is not expected). These minor modifications ensure that the algorithm can adapt to level changes in the BCG signal caused by different means, e.g. the respiratory activity.

### C. DESCRIPTION OF OBJECTIVE IMAGE QUALITY EVALUATION

In order to evaluate the influence of different triggering methods on the quality of the resulting images, we carried out an objective evaluation of images using Blind/Referenced Image Quality Evaluator (BRISQUE), Naturalness Image Quality Evaluator (NIQE), and Perception Based Image Quality
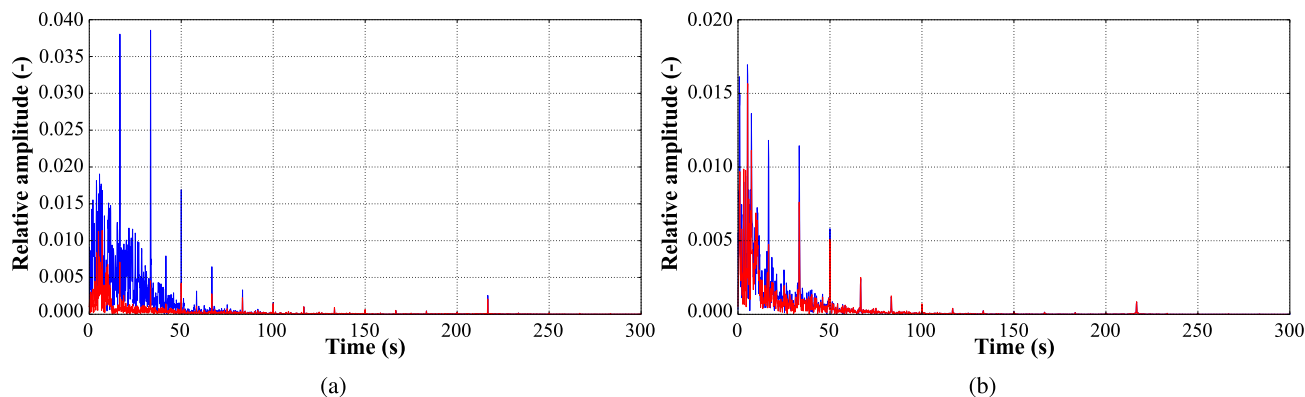
**FIGURE 8.** The spectrum of BCG signal (red) and interference (blue) (a) at TF sequence, (b) at PSIR sequence.

Evaluator (PIQE). BRISQUE is based on the calculation of the no-reference image quality score. The lower the value of the result, the better the quality of the image evaluated. This ranking algorithm works in a spatial domain and does not calculate distortion-specific features, such as ringing, blur, or blocking. BRISQUE uses scene statistics of locally normalized luminance coefficients to assess the level of image quality that can be reduced due to the presence of distortions. It basically uses the natural scene statistics model and evaluates 'naturalness' using the parameters of that model. This algorithm is very simple and provides much more statistically meaningful values than, for example, the calculation of signal-to-noise ratio and structural similarity index [47], [48].

NIQE, as well as BRISQUE, is used to evaluate image quality by calculating the no-reference image quality score. The lower the value of the result, the better the quality of the image evaluated. This ranking algorithm is based on the construction of 'quality aware' statistical elements based on a simple space domain natural scene statistics model. Individual elements are estimated using natural and undistorted images. At first glance, it is clear that both NIQE and BRISQUE use the natural scene statistics model. However, NIQE uses only natural scene statistics from the corpus of natural images. This means that the BRISQUE algorithm is limited to a particular type of distorted images on which it was built, and the NIQE algorithm is not limited to a specific type of images. The big advantage of this NIQE algorithm is that it achieves comparable statistical values with other algorithms that require learning on a large number of databases of human decisions about distorted images [49].

Again, PIQE, as well as BRISQUE and NIQE, is used to evaluate image quality by calculating the no-reference image quality score. The lower the value of the result, the better the quality of the image evaluated. Again, the PIQE algorithm attempts to quantify the distortion of images without reference. It is based on extracting local features to estimate the quality of the images. To imitate human behaviour, the image quality estimation is conducted using only perceptually significant spatial regions. Selecting elements allows you to generate a distortion map using blocks. PIQE is a competitive algorithm that has low computational complexity even though it works in blocks [50], [51].

### D. DESCRIPTION OF ADAPTIVE CANCELLING SYSTEM

The embodiment of the pneumatic sensor according to Fig. 4 uses pacient circuit 4a for the actual BCG measurement. Unfortunately, this circuit senses the undesirable mechanical and acoustic interference caused by MR along with the desired BCG signal. The proposed concept also includes reference circuit 4b which is located outside the patient's body and, therefore, senses only unwanted mechanical and acoustic interference without the desired BCG signal.

The simplest approach to eliminate the interference is direct subtraction of the signal acquired from the reference circuit, which contains only unwanted components from the patient circuit containing both unwanted components and the desired BCG signal. However, this procedure cannot be used in clinical practice since the interfering signals sensed by the reference circuit differ from the interference signals sensed by the pacient circuit. This is caused mainly by the effects of an unknown MRI environment (signal distortion due to interference, delay, etc.).

Linear filtering cannot be used to eliminate unwanted interference either, as the useful (BCG) and interfered signal spectra overlap each other, see Fig. 8. Another significant problem is that the interference spectrum varies for different sequences and is, therefore, variable over time. In addition, the spectrum parameters are influenced by the load on the pneumatic sensor (varying weight and patient area).

We are facing the problem that the filter should work in an unknown environment in which the preliminary identification is difficult, or it is a time-varying environment whose development cannot be predicted in the future. In such a case, the values of the optimum filter coefficients change over time and adaptive filtering is appropriate for proper adjustment [53]–[55].

There are a number of algorithms that can be used to eliminate the interference, e.g. adaptive filters with stochastic gradient MSE adaptation (LMS, NLMS, VSLMS, etc.) [56]–[58], adaptive filters with recursive optimal
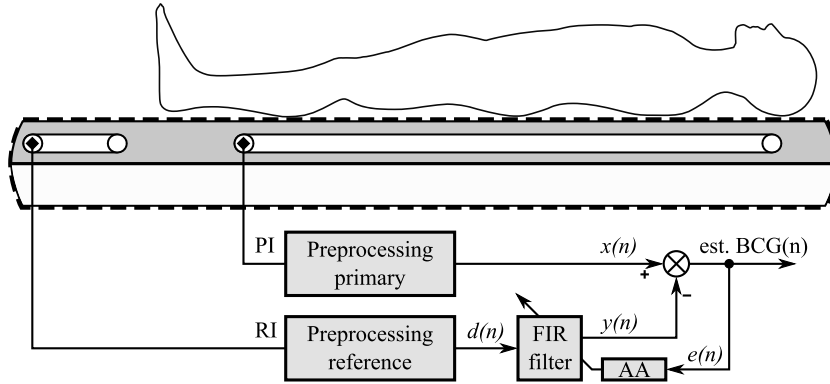
**FIGURE 9.** A simplified principle diagram of the adaptive system to eliminate mechanical and acoustic interference.

adaptation (RLS, FTF, etc.) [59]–[61], Kalman filtering [62], adaptive linear neuron ADALINE [63], etc., soft-computing methods (e.g. artificial neural networks, fuzzy logic, fuzzy-neural networks (e.g. ANFIS), genetic algorithms, etc.) [64]–[66]. Furthermore, non-adaptive processing methods based on the principles of blind separation of BSS resources (e.g. PCA - principal component analysis, ICA - independent component analysis, SVD - singular value decomposition, etc.) [67]–[70], wavelet transforms [70], [71], spectral subtraction method [70], [72], etc. Unfortunately, many methods are unusable due to the extreme requirements for FPGA implementation speed and complexity. For this reason, a stochastic gradient adaptation was used where the least mean squares algorithm (LMS) was chosen [53], [54].

The simplified diagram according to Fig. 9 shows two signal sources that are isolated from each other and operate autonomously:

- Primary input: the signal sensed is a mixture of a useful BCG signal (the source of which is the patient's heart) and interference that can be of various origins.
- Reference input: the signal sensed is only interference without a useful BCG signal.

A linear transversal FIR filter was used as a basis of the adaptive filter and an adaptive LMS algorithm was used to adapt the filter coefficients (Fig. 9 - AA block). The FIR filter coefficients of this system are updated by the LMS training algorithm, which is based on a feedback error signal, which equals to the desired signal. Thus, it can be said that the system adapts in real time, so that we can subtract interfering signal $y(n)$ from signal $x(n)$, and the required est. $BCG(n)$ signal remains. Each iteration of the LMS algorithm requires 3 different steps to be performed, in the order given. First, the FIR output value of $y(n)$ is calculated according to equation (1), valid in $R$:

$$y(n) = \overrightarrow{w}^{\mathrm{T}}(n) \cdot \overrightarrow{x}^{\mathrm{T}}(n) = \sum_{i=0}^{N} w_i(n) \cdot x(n-i). \qquad (1)$$

The value of the estimated error signal $e(n)$ is then calculated according to equation (2) in $R$, as follows:

$$e(n) = d(n) - y(n). \qquad (2)$$

**TABLE 1.** General information on the subjects tested.

| Subject parameters | (N = 10) |
|---|---|
| Age, years | 42±21 |
| Females, n (%) | 4 (40) |
| Males, n (%) | 6 (60) |
| Height, cm | 166±19 |
| Weight, kg | 75±23 |
| BMI, kg/m2 | 24.6±3.4 |
| Systolic blood pressure, mmHg | 117±27 |
| Diastolic blood pressure, mmHg | 71±13 |

Finally, the vector weight values $\overrightarrow{w}(n)$ of the corresponding FIR filter are updated with respect to the following iteration according to equation (3), valid in $R$.

$$\overrightarrow{w}(n+1) = \overrightarrow{w}(n) + 2 \cdot \mu \cdot e(n) \cdot \overrightarrow{x}(n),$$
$$\overrightarrow{w}(n+1) = \overrightarrow{w}(n) + k_\mu \cdot e(n) \cdot \overrightarrow{x}(n),$$
$$\overrightarrow{w}(n+1) - \overrightarrow{w}(n) = 2 \cdot \mu \cdot [d(n) - y(n)] \cdot \overrightarrow{x}(n)$$
$$= \delta \overrightarrow{h}(n) \quad \forall n \in Z^+,$$
$$\overrightarrow{h}(n+1) = \overrightarrow{h}(n) + \delta \overrightarrow{h}(n) \quad \forall n \in Z^+. \qquad (3)$$

The LMS algorithm implementation can be summarized in $R$ as follows:

$$BEGIN \ \ \overrightarrow{w}(n=0) = \overrightarrow{0},$$
$$FOR \quad (n = 1, 2, \ldots, N):$$
$$y(n) = \overrightarrow{w}^{\mathrm{T}}(n) \cdot \overrightarrow{x}(n),$$
$$e(n) = d(n) - y(n),$$
$$\overrightarrow{w}(n+1) = \overrightarrow{w}(n) + k_\mu \cdot e(n) \cdot \overrightarrow{x}(n). \qquad (4)$$

For a detailed description of the LMS algorithm derivation see [56] or [58].

## III. RESULTS OF THE PILOT PRE-CLINICAL STUDY

The experimental measurements performed on the pneumatic BCG sensor within the Siemens Prisma 3T MR scan were conducted on a sample of 10 healthy subjects (6 males and 4 females) upon written consent and upon the approval of the Ethics Committee. The age range of the subjects was from 21 to 63 years, the weight ranged from 47 to 104 kg. All general information on the subjects tested is summarized in Table 1.

**TABLE 2.** The parameters of the MR sequences used for cardiac triggering.

| Sequence | Field of view (mm) | Time to echo (ms) | Acquisition time (min:sec) | Inversion time (ms) | Slice thickness (mm) |
|---|---|---|---|---|---|
| TRufisp | 340×284 | 1.4 | 12 sec | - | 6 |
| PSIR | 350×263 | 1.5 | 11 sec | 270 | 8 |



(a)  (b)  (c)

**FIGURE 10.** The resulting images (subject 1 - F) using the Truefisp sequence (Siemens): (a) TF - ECG, (b) TF - PPG, (c) TF - BCG.



(a)  (b)  (c)

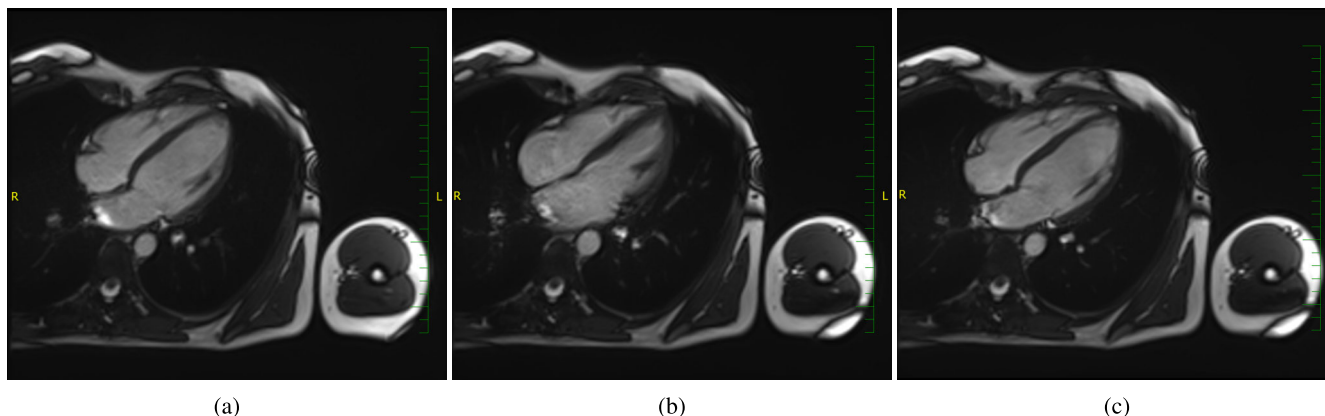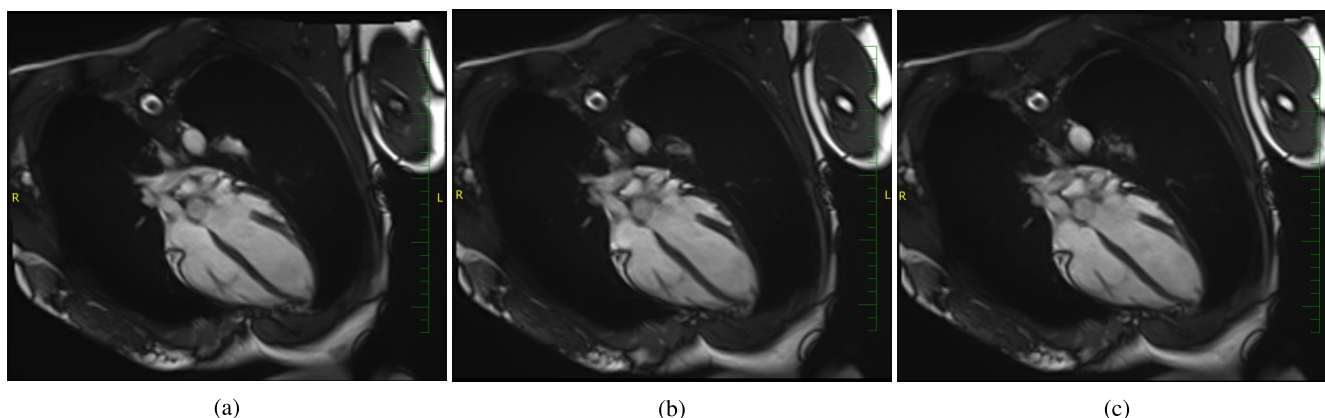**FIGURE 11.** The resulting images (subject 6 - M) using the Truefisp sequence (Siemens): (a) TF - ECG, (b) TF - PPG, (c) TF - BCG.

The pilot research compares the novel FPGA-based pad monitoring system for cardiac triggering using BCG with clinically used systems based on ECG and PPG. The individual parameters of the MR sequences used for cardiac triggering are shown in Table 2 below.

The applicability of the proposed BCG system was analyzed using subjective as well as objective methods:

- **A**: Subjective evaluation of the images by 10 experts based on a blind questionnaire - subjective comparison of BCG vs. ECG vs. PPG images, (10 subjects, two sequences (TF, PSIR), three-mode triggering, grade 1 to 3 - including the possibility of matching). The study presents images of four subjects ()two best and two worst subjects based on the statistical evaluation) for 2xTRUE FISP (Free Induction Decay Steady-State Precession) and 2xPSIR (Phase Sensitive Inversion Recovery) sequences. The examples include one female subject and one male subject, see Fig. 10 to Fig. 13. Furthermore, objective evaluation of images using

BRISQUE, NIQE, PIQE was performed, see Table 3, Fig. 14, and Fig. 15.
- **B**: Objective evaluation of ECG vs. BCG based on R-R or J-J detection to determine heart rate variability.
- **C**: The efficiency of the adaptive system for reducing acoustic and mechanical disturbances.

## A. COMPARISON OF ECG vs. PPG vs. BCG IMAGES FOR TRUEFISP (SIEMENS) AND PSIR (SIEMENS) SEQUENCES

Figure 10a (subject 1 - F) shows the resulting image using the Truefisp (Siemens) sequence - a balanced echo to illustrate a dynamic event - a moving organ. This image was created using the standard triggering using the ECG signal supplied by the manufacturer. A 4-chamber projection for assessing the movement of the walls of the four heart chambers is apparent. This image shows a sharp contour of the left ventricle wall, a good depiction of the papillary muscles. Figure 10b is the resulting image using PPG pulse triggering by means
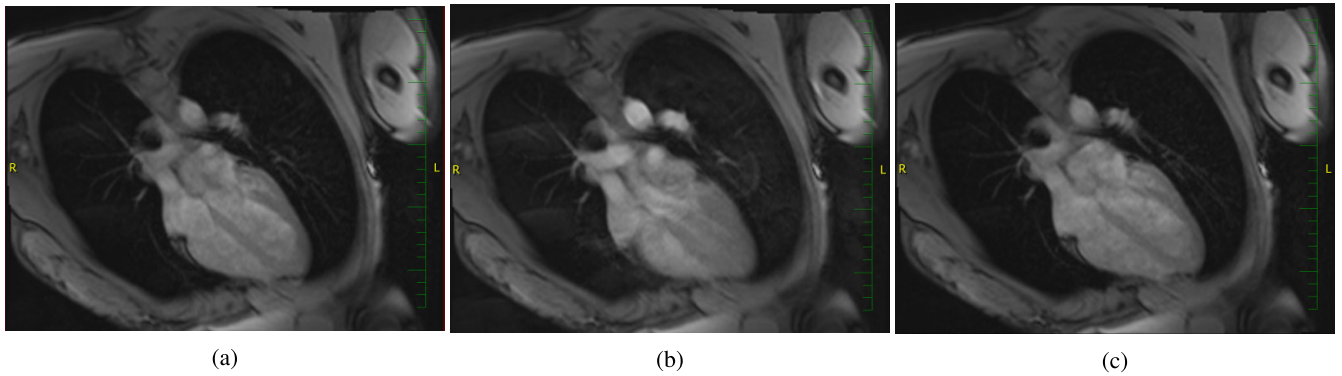
**FIGURE 12.** The resulting images (subject 2 - F) using the PSIR sequence (Siemens): (a) PSIR - ECG, (b) PSIR - PPG, (c) PSIR - BCG.
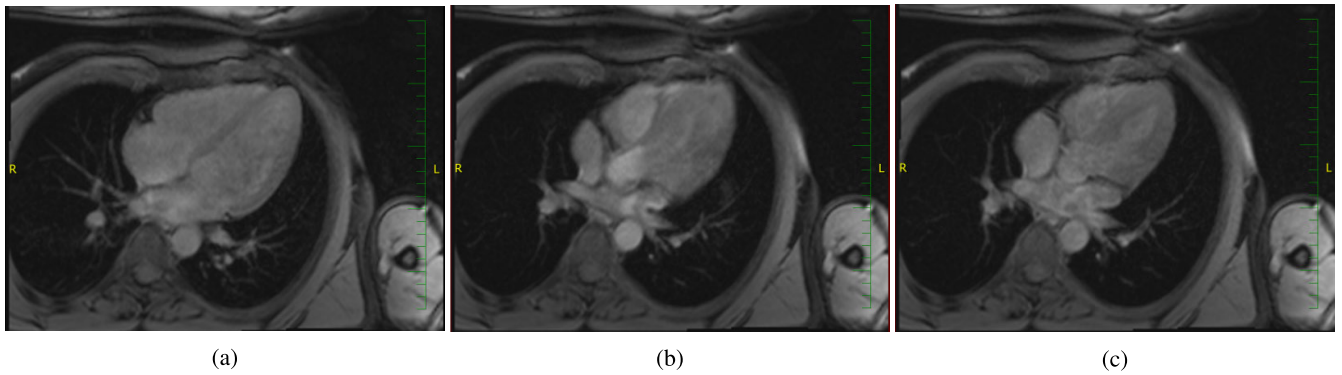


**FIGURE 13.** The resulting images (subject 8 - M) using the PSIR sequence (Siemens): (a) PSIR - ECG, (b) PSIR - PPG, (c) PSIR - BCG.

**TABLE 3.** Summarization of objective evaluation using Truefisp sequence (Siemens) sequences.

| Subject | ECG | PPG | BCG | ECG | PPG | BCG | ECG | PPG | BCG |
|---------|-----|-----|-----|-----|-----|-----|-----|-----|-----|
| | BRISQUE | | | NIQE | | | PIQE | | |
| 1 | 43.6 | 40.4 | 45.3 | 18.9 | 18.9 | 18.9 | 57.3 | 53.6 | 62.3 |
| 6 | 36.4 | 39.1 | 35.9 | 18.9 | 18.9 | 18.9 | 55.3 | 72.3 | 57.6 |

of a finger optical detector. The resolution is lower due to movement artifacts; there is a slight shift in the cardiac cycle phase - the left ventricle is already in the contraction phase. Figure 10c is the resulting image using the BCG sensor tested (triggering). The image is comparable to the image generated by ECG triggering (Fig. 10a). A comparable phase of the heart cycle - end-diastole - is visible; the spatial resolution of the kinematic sequence is also comparable to the standard execution by ECG triggering. Rendering of anatomical structures is adequate.

Figure 11a (subject 2 - M) shows the resulting image using the Truefisp (Siemens) sequence - triggering by ECG curve supplied by the manufacturer. In the 4-CH projection, the wall of the left chamber, as well as the papillary muscle structure, are well evaluated. Figure 11b is the resulting image of the Truefisp sequence (Siemens); in this subject, PPG triggering is compared to classical ECG triggering; the cardiac wall structures, as well as the papillary muscles, are sharp. Figure 11c is the resulting image using the BCG sensor tested (triggering). The fugure shows a good resolution of both the chamber and the papillary muscles;

the moving blood-solid wall of the chamber interface is relatively sharp.

Figure 12 (subject 1 - F) is the resulting image using the PSIR sequence (Siemens), which is performed post-contrast (scarring) as standard, is performed natively here. Figure 12a is the resulting image using ECG triggering. In the 4-CH projection, the wall is well detectable, the contours of the heart sections are sharp. In Fig. 12b, the PSIR sequence is performed using PPG triggering, there is an evident phase delay compared to ECG and BCG triggering, fuzzy heart wall contours. In Fig. 12c, a PSIR sequence with BCG triggering is performed; it is fully comparable to an image using ECG BCG; we can easily differentiate between blood-filled and myocardium-formed structures whose interface is sharp.

Figure 13a is the resulting image using a PSIR sequence (Siemens), native to subject 3. In the image (Fig. 13a) taken by ECG triggering, good image quality is evident with a well-differentiated boundary of the structures filled with blood and solid tissue. Figure 13b shows a clear phase shift of the cardiac cycle - the heart is contracted in the systole - there is no good differentiation of the fluid-filled chamber
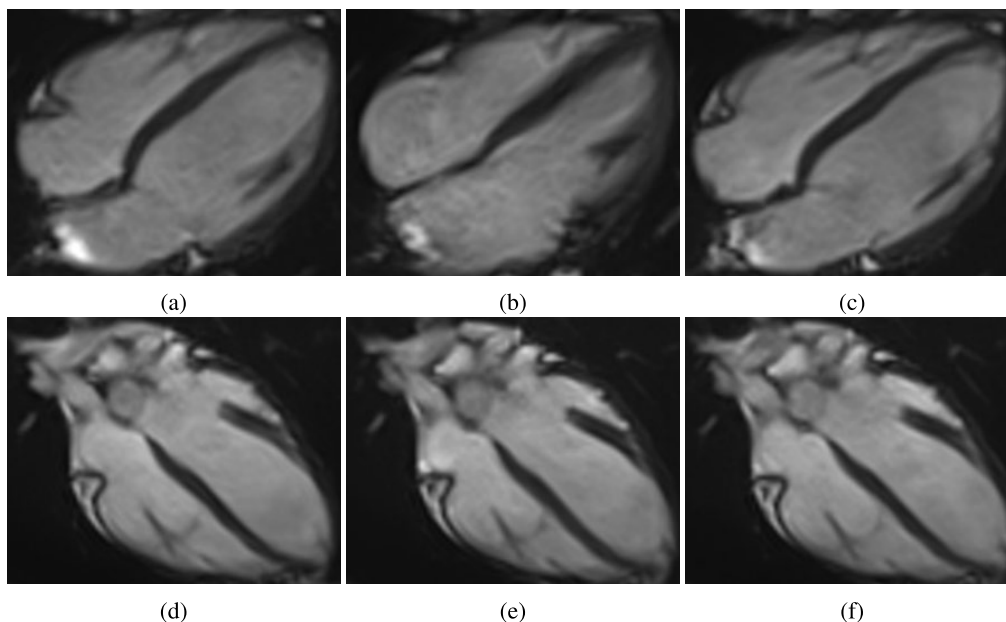
**FIGURE 14.** Images for objective evaluation using Truefisp sequence (Siemens) sequences: subject 1: (a) TF - ECG, (b) TF - PPG, (c) TF - BCG; subject 6: (d) TF - ECG, (e) TF - PPG, (f) TF - BCG.
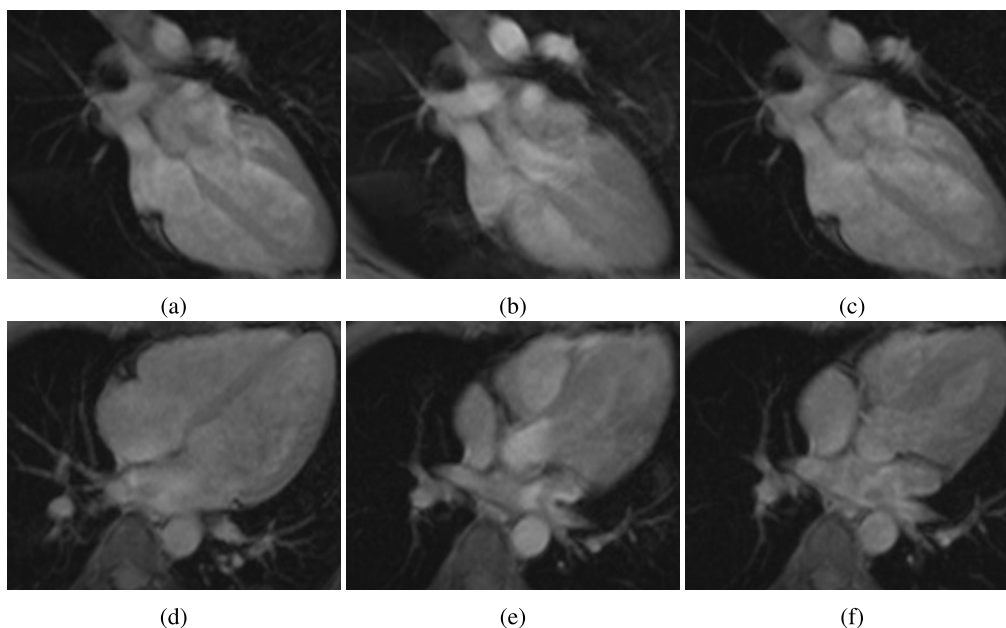


**FIGURE 15.** Images for objective evaluation using PSIR sequence (Siemens) sequences: subject 2: (a) PSIR - ECG, (b) PSIR - PPG, (c) PSIR - BCG; subject 8: (d) PSIR - ECG, (e) PSIR - PPG, (f) PSIR - BCG.

and its wall. In Fig. 13c, taken by BCG triggering, there is still evident a phase shift towards the cardiac action - the heart is already contracting in the systole, but there is a good differentiation between the fluid-filled chamber and the solid tissue of the heart muscle.

Furthermore, images were also prepared for processing objective evaluation of images using BRISQUE, NIQE, and PIQE, see Fig. 14 and Fig. 15. Here, clinically significant areas were selected to eliminate distortion by redundant areas.

The results of objective evaluation are summarized in Table 3 and Table 4. It can be stated that the diagnostic quality of the image does not correlate exactly with the image quality by means of the methods used. Nevertheless, no value deviates significantly, see Table 3 and Table 4; it can be concluded that this analysis has shown the equivalence of the results achieved in terms of image quality. The results show that these methods are unable to evaluate the diagnostic quality of the resulting images, see the comparison of the objective

**TABLE 4.** Summarization of objective evaluation using PSIR sequence (Siemens) sequences.

| Subject | ECG | PPG | BCG | ECG | PPG | BCG | ECG | PPG | BCG |
|---------|-----|-----|-----|-----|-----|-----|-----|-----|-----|
| | BRISQUE | | | NIQE | | | PIQE | | |
| 2 | 40.8 | 42.3 | 40.9 | 18.9 | 18.9 | 18.9 | 42.0 | 50.3 | 45.8 |
| 8 | 37.6 | 40.9 | 36.3 | 18.9 | 18.9 | 18.9 | 44.1 | 42.9 | 41.8 |

**TABLE 5.** Results of the evaluation performed by doctors.

| Subject | TF - ECG | TF - PPG | TF - BCG | PSIR - ECG | PSIR - PPG | PSIR - BCG |
|---------|----------|----------|----------|------------|------------|------------|
| 1 | 2.2 | 1.7 | 1.3 | 2.0 | 2.1 | 1.3 |
| 2 | 1.2 | 1.4 | 1.3 | 1.1 | 2.2 | 1.9 |
| 3 | 1.1 | 1.3 | 1.1 | 1.3 | 1.9 | 1.1 |
| 4 | 2.0 | 1.5 | 1.2 | 1.7 | 2.8 | 1.4 |
| 5 | 1.0 | 1.2 | 1.1 | 1.0 | 3.0 | 1.2 |
| 6 | 1.5 | 1.8 | 1.4 | 1.5 | 2.7 | 1.5 |
| 7 | 1.2 | 1.2 | 1.2 | 1.1 | 2.1 | 1.2 |
| 8 | 1.0 | 1.2 | 1.2 | 1.0 | 2.0 | 1.7 |
| 9 | 1.1 | 2.0 | 1.4 | 1.8 | 2.5 | 1.6 |
| 10 | 1.3 | 1.4 | 1.2 | 1.0 | 2.5 | 1.1 |
| Mean | 1.36 | 1.47 | 1.24 | 1.35 | 2.38 | 1.4 |
| Diagnostic Quality: 1 to 3 (1 = best, 2 = medium, 3 = poor) Mean - 10 experts | | | | | | |

evaluation and blind subjective test in Table 3, 4 and 5, respectively. According to the experts involved in this pilot study, the images that achieved worse results in objective evaluation using BRISQUE, NIQE, and PIQE are more valuable from the diagnostics perspective than images that achieve better results.

Table 5 summarizes the results of the blind test performed by experts. 10 clinicians were involved in the blind test. Each of them received images from each of the subjects tested. For the TF and PSIR sequences, they each received three images (i.e. a total of 60 images) where triggering was performed by means of three methods tested, i.e. ECG, PPG and BCG. The experts did not have information on how the pictures were taken. They performed the evaluation by giving points from 1 to 3 (1 means the best); an agreement was acceptable (i.e. the same diagnostic quality).

According to the interobserver study, it is clear that images generated by ECG and BCG triggering are comparably beneficial to the physician making a diagnosis; BCG triggering is evaluated as more beneficial in terms of kinematic sequence results.

## B. COMPARISON BETWEEN ECG AND BCG BASED SYSTEMS

As part of our research, we carried out a comparison of the BCG signal acquired by our new sensor and the "gold standard" ECG signal based monitoring system on the statistical assessment of the peaks detected in these signals and the heart rate traces determined using the peaks detected. We considered ECG as a reference or the "gold standard" because ECG-based systems are natively used for triggering of MRI sequences and they are also the most prevalent triggering method in clinical practice. Semi-automatic evaluation of all detected R peaks was performed to ensure that the ECG signal can be really used as a reference. Additionally, we selected only those intervals where the quality of the ECG signal was high (patient lied still, and no MRI sequence

was running) and R waves were not distorted by any kind of interference.

Datasets for statistical assessment were acquired from 10 different patients where 6 of them were men and 4 women, aged from 21 to 63 years. All patients were in good health and the tests were approved by the ethics committee. The average time duration of the datasets analysed was 15 minutes, wherein the range was from 12 to 18 minutes. In the first part of our statistical assessment, we employed Bland-Altman analysis, which is used to compare results of two independent measurements of the same variable. Details about this method are described in our previous research [36] and in [52]. Examples of two best and two worst results are depicted and described in Fig. 16 to Fig. 19 and the results for all subjects are shown in columns 5 and 6 in Table 4.

The second part of our statistical assessment is based on classification of significant peaks detected in the BCG signal corresponding to R peaks detected in the ECG signal. Before the process of peak classification, both signals had to be aligned in a time domain to compensate for the delay of the BCG to ECG signal. This delay of a fixed number of samples is caused by biological processes in the human body and by the signal propagation through the sensor and the tubing system. The peak classification process aims to categorize the peaks detected as false positive (FP), false negative (FN) or true positive (TP). The outputs of the peak classification obtained are used to calculate four statistical parameters determining the performance of peak detection in the BCG signal in comparison to peaks detected in the reference ECG signal. These parameters are sensitivity (SE), positive predictive value (PPV), Accuracy (ACC) and F1 score. The process of peak classification, formulas and descriptions of the statistical parameters mentioned is described in detail in our previous research [36]. The results of the peak classification process are shown in Table 6.

Table 6 summarizes the results of statistical assessment of peak detection for 10 subjects, where the BCG signal
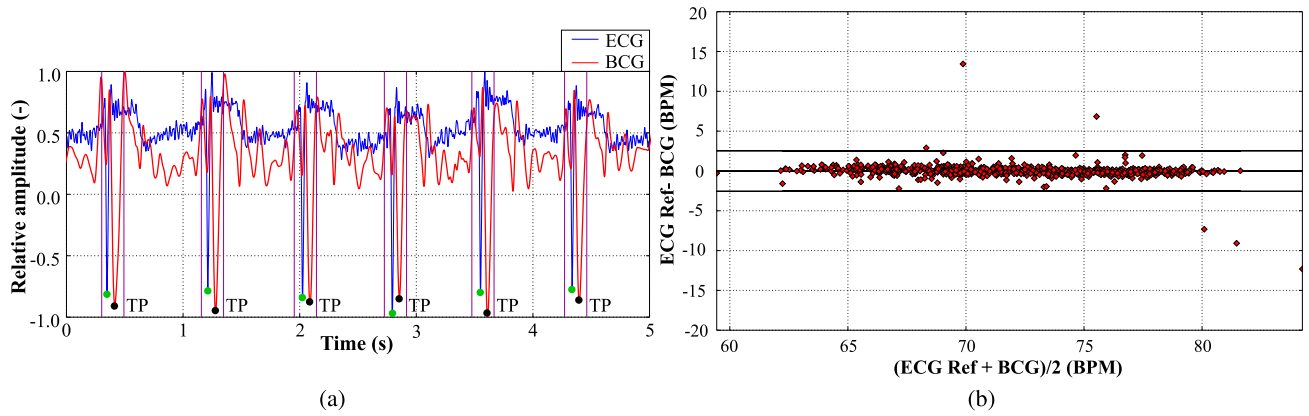
**FIGURE 16.** Comparison for subject 1 - F: (a) a sample of ECG and SSG waveform; (b) Bland-Altman analysis of ECG vs. BCG.
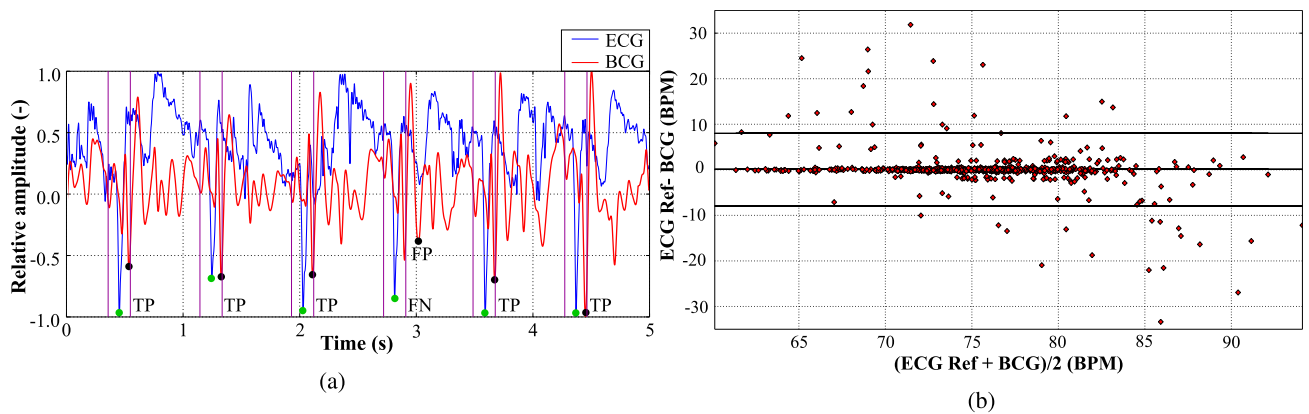


**FIGURE 17.** Comparison for subject 6 - M: (a) a sample of ECG and SSG waveform; (b) Bland-Altman analysis of ECG vs. BCG.
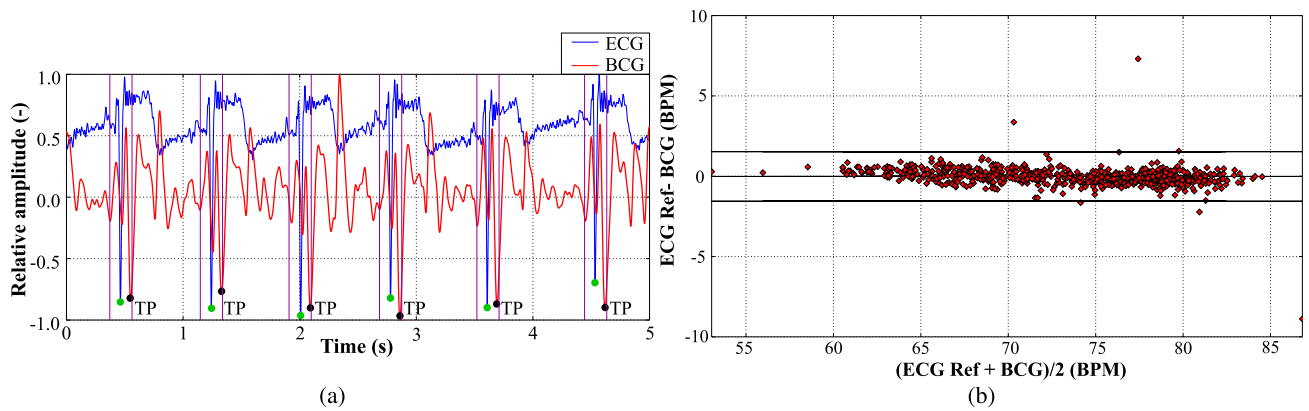


**FIGURE 18.** Comparison for subject 2 - F: (a) a sample of ECG and SSG waveform; (b) Bland-Altman analysis of ECG vs. BCG.

captured by our sensor was compared with the conventional ECG reference signal. The results of Bland-Altman analysis are shown in columns denoted as $\mu$ and $1.96\sigma$. Two best and two worst results are highlighted in bright green and bright red colours, respectively. Bland-Altman analysis indicates only minor difference bias ($\mu$= -0.18 bpm) for subjects 3 and 8. The difference bias of the remaining subjects is practically equal to zero (-0.07 bpm and less). These results do not indicate any significant systematic error in the peak

detection process. Lines of agreement ($1.96\sigma$) are ranging from 1.18 bpm to 7.98 bpm, the results of more than half of the subjects fall above 5 bpm. Higher values of the lines of agreement indicate a higher variance of the samples in dataset. This is mainly caused by the presence of outliers in the heart rate values determined, as shown in Fig. 17 and Fig. 19. Outliers are results of movement artifacts caused by the motion of the subject during the measurement. Frequency components of the most typical motion artifacts occupy the
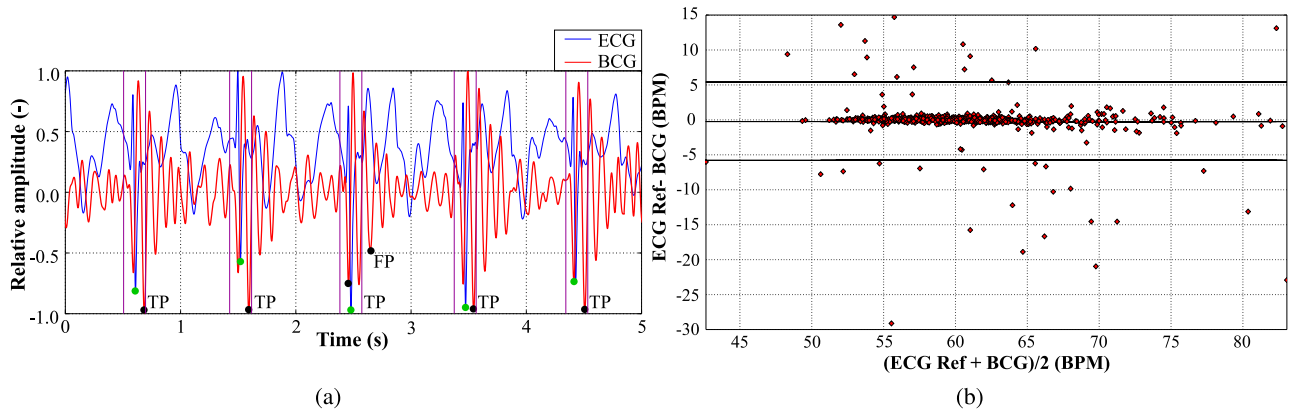
**FIGURE 19.** Comparison for subject 8 - M: (a) a sample of ECG and SSG waveform; (b) Bland-Altman analysis of ECG vs. BCG.

**TABLE 6.** Summarization of the results achieved on all subjects tested.

| Subject | TP | FP | FN | Mean | Std | Acc | Sens | PPV | F1 |
|---|---|---|---|---|---|---|---|---|---|
| 1 | 707 | 3 | 3 | -0.02 | 1.9 | 99.15 | 99.57 | 99.57 | 99.57 |
| 2 | 749 | 1 | 1 | -0.02 | 1.18 | 99.73 | 99.86 | 99.86 | 99.86 |
| 3 | 598 | 16 | 15 | -0.18 | 6.32 | 95.07 | 97.55 | 97.39 | 97.47 |
| 4 | 617 | 7 | 8 | 0.03 | 5.72 | 97.62 | 98.72 | 98.87 | 98.79 |
| 5 | 729 | 14 | 14 | 0.02 | 5.89 | 96.3 | 98.11 | 98.11 | 98.11 |
| 6 | 752 | 31 | 32 | 0.04 | 7.98 | 92.26 | 95.71 | 96.04 | 95.97 |
| 7 | 659 | 8 | 8 | 0.02 | 4.48 | 97.62 | 98.8 | 98.8 | 98.8 |
| 8 | 672 | 25 | 25 | -0.18 | 5.6 | 93.07 | 96.41 | 96.41 | 96.41 |
| 9 | 939 | 8 | 8 | -0.01 | 3.37 | 98.32 | 99.15 | 99.15 | 99.15 |
| 10 | 925 | 27 | 27 | -0.07 | 5.55 | 94.48 | 97.16 | 97.16 | 97.16 |
| **Total** | **7347** | **140** | **141** | **-** | **-** | **96.31** | **98.11** | **98.13** | **98.12** |

same frequency band as the BCG signal which makes their removal by means of conventional FIR or IIR filters nearly impossible. The advanced signal processing methods (e.g. based on adaptive filtering using a reference signal containing the noisy signal only) would have to be employed [36]. It should be noted that motion artifacts are not a problem during MRI since the patient is required to lie as still as possible, otherwise the resulting MRI images are blurry and distorted. The results of peak classification are consistent with Bland-Altman analysis with ACC values ranging from 92.2% to 99.8% and F1 score ranging from 95.9% to 99.8% with the results of more than half of the subjects being above 95%. The last row the of Table 3 contains the results of peak classification obtained from all subjects measured.

In total, 748 peaks (heart beats) were detected, with 7,347 correctly identified as TP peaks, 140 incorrectly detected as FP peaks, and 106 missed peaks (FN). For all subjects, the total accuracy reached 96.31% and F1 score reached 98.18%. In medical fields, the results are considered accurate if the values of the ACC, SE, PPV, and F1 parameters exceed 95%, which was achieved in case of more than half of the subjects. The results prove that the BCG signal captured by our new sensor can be used as a substitute for ECG signal during MRI exam with reliability of 97%.

### C. ADAPTIVE NOISE CANCELLING

From Fig. 20, it is evident that both circuits of the pneumatic system detect mechanical and acoustic interference. Further,

it is also apparent that the useful BCG signals in Fig. 20a is significantly below the superimposed interference level. Such a signal is not usable for triggering, see Fig. 21. Figure 21a shows an image using ECG triggering, Fig. 21b shows an image using the raw BCG signal from the measuring circuit. The detection system was unable to identify any relevant triggering points.

Figure 21a shows sharp solid tissue-fluid transitions, the motion is sharp. From the movement perspective, Fig. 21b is blurred, not well-targeted in the phase of cardiac movement - there are signs of ventricular contraction, there is evident the impossibility of accurate fluid-solid tissue differentiation, especially in the area of papillary muscles.

Figure 20a shows a selected part of the input signal to be analyzed acquired from the pacient circuit during the TF sequence (4a), and Fig. 20b shows the corresponding waveform sensed by the reference circuit (4b).

Figure 22a shows a selected part of the signal to be analyzed sensed by the pacient circuit during the PSIR sequence, and Fig. 22b shows the corresponding waveform from the reference circuit. Even during this sequence, the presence of mechanical and acoustic interference is evident. This is a lower level of interference than in the previous case (Fig. 20), however, the data from pacient circuit Fig. 22a is not usable for triggering.

Figure 23a shows an image using ECG triggering (PSIR) and Fig. 23b shows an image using the raw BCG signal from the pacient circuit. The detection system was unable to
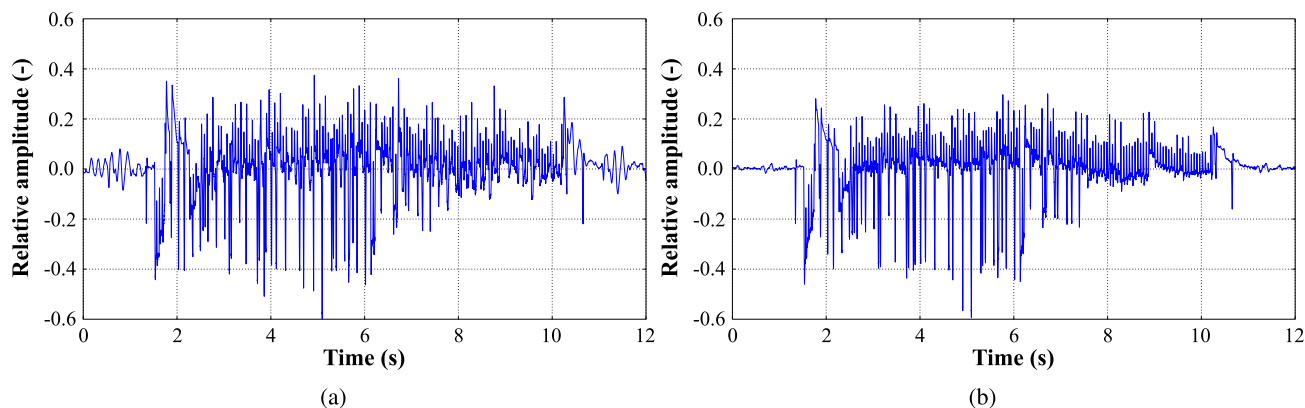
**FIGURE 20.** A selected part of the input signal during the TF sequence: (a) the pacient circuit; (b) the reference circuit.
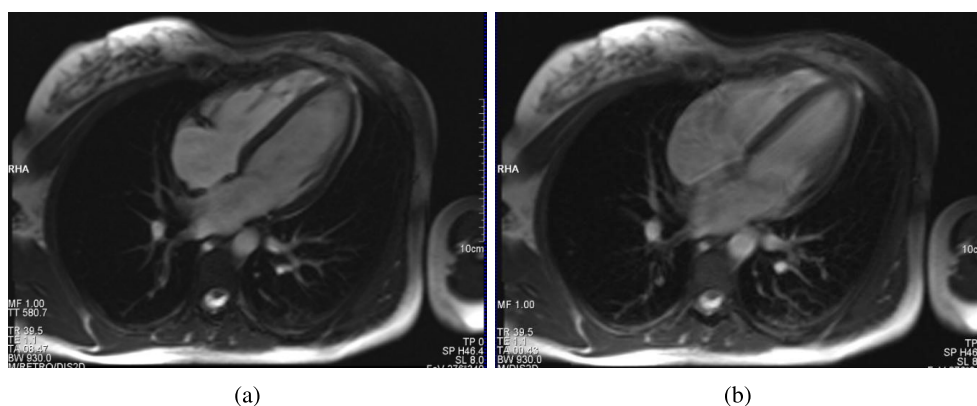


**FIGURE 21.** The resulting images using the Truefisp sequence (Siemens): (a) TF - ECG, (b) TF - BCG without processing, i.e. row data.
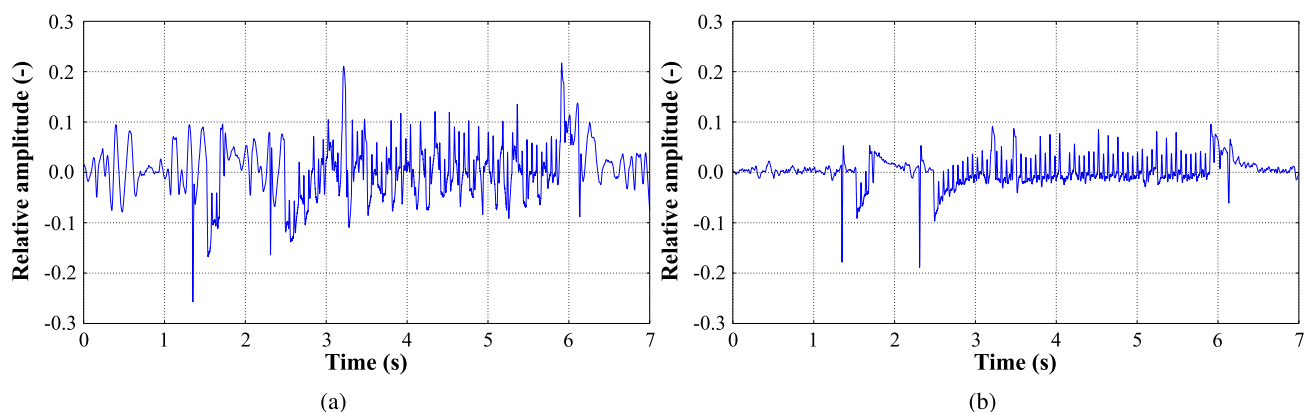


**FIGURE 22.** A selected part of the signal during the PSIR sequence: (a) the pacient circuit; (b) the reference circuit.

identify any relevant triggering points. In Fig. 23a, the view of the heart sections is slightly modified by movement artifacts of the blood flowing, the heart is at its maximum dimension - at the end of the filling phase. Figure 23b shows a phase shift in the cardiac activity - the heart is already contracting, the sharpness of the anatomical structures in the atrium area is sufficient, the left ventricular wall contour is blurred due to the contraction.

Figure 24 shows the results of adaptive filtering. Figure 24a represents the original signal measured using the pacient circuit during the TF sequence and Fig. 24b represents the signal after filtration using the adaptive LMS system during the TF sequence. Figure 24c then represents the signal before filtration during the PSIR sequence and Fig. 24d represents the signal after filtration using the adaptive LMS system during the PSIR sequence.
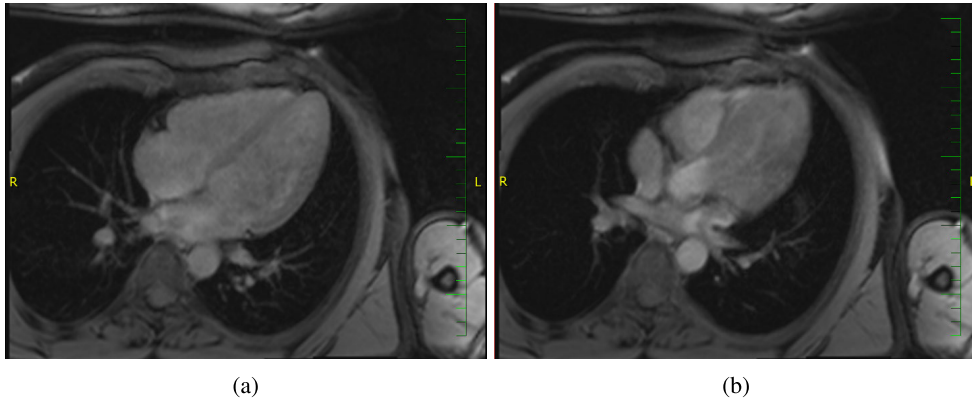
(a)                                              (b)

**FIGURE 23.** The resulting images using the PSIR sequence (Siemens): (a) TF - ECG, (b) TF - BCG without processing, i.e. row data.
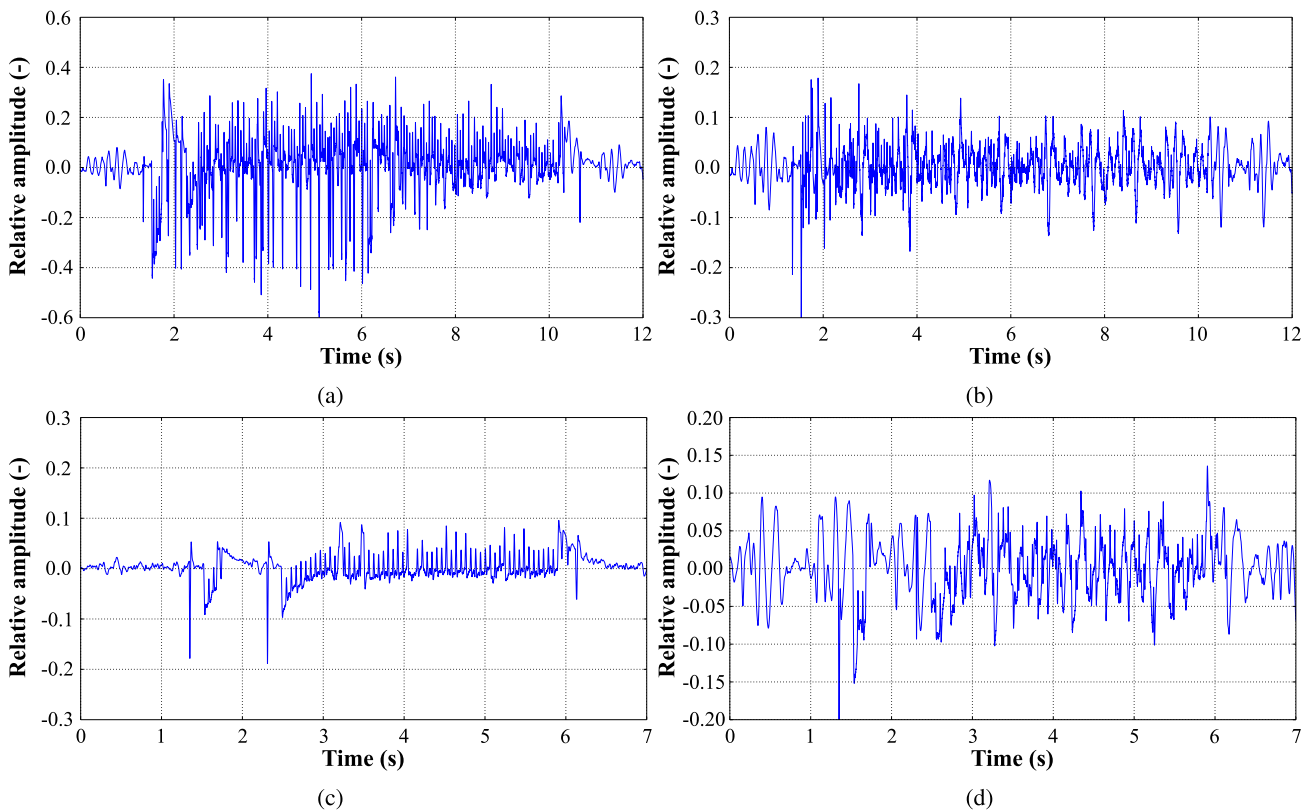


(a)

(b)

(c)

(d)

**FIGURE 24.** Results of adaptive filtering using the LMS algorithm in terms of: (a) BCG signal before filtration - TF; (b) BCG signal after adaptive filtering - TF; (c) BCG signal before filtering - PSIR; (d) BCG signal after adaptive filtering - PSIR.

From the results presented in Fig. 24, it is apparent that adaptive filtering is very effective in extracting BCG signals from the proposed pneumatic sensor. The advantage of the concept used is its easy implementation on FPGA and, above all, adaptability in various sequences (e.g. TF vs. PSIR).

Before the adaptively processed signals were used for triggering, they were finally processed using a low-pass IIR filter of the second order of Butterworth approximation with a cut-off frequency of 15 Hz. Figure. 25 and Fig. 26 interpret the processing results from the actual triggering perspective. Obviously, BCG processing has a major effect on image quality. In the figures, two areas are

colour-coded, red being the area where the triggering is not working properly and green being the area where the triggering is correct.

## IV. DISCUSSION

This pilot pre-clinical study confirmed the functionality of the novel FPGA-based pad monitoring system for cardiac triggering using ballistocardiography designed and patented by the authors. The primary advantage of the proposed system is the part part located under the patient's body. A patented pneumatic pad prototype was used in this pilot pre-clinical study. The advantage of the concept used is portability.
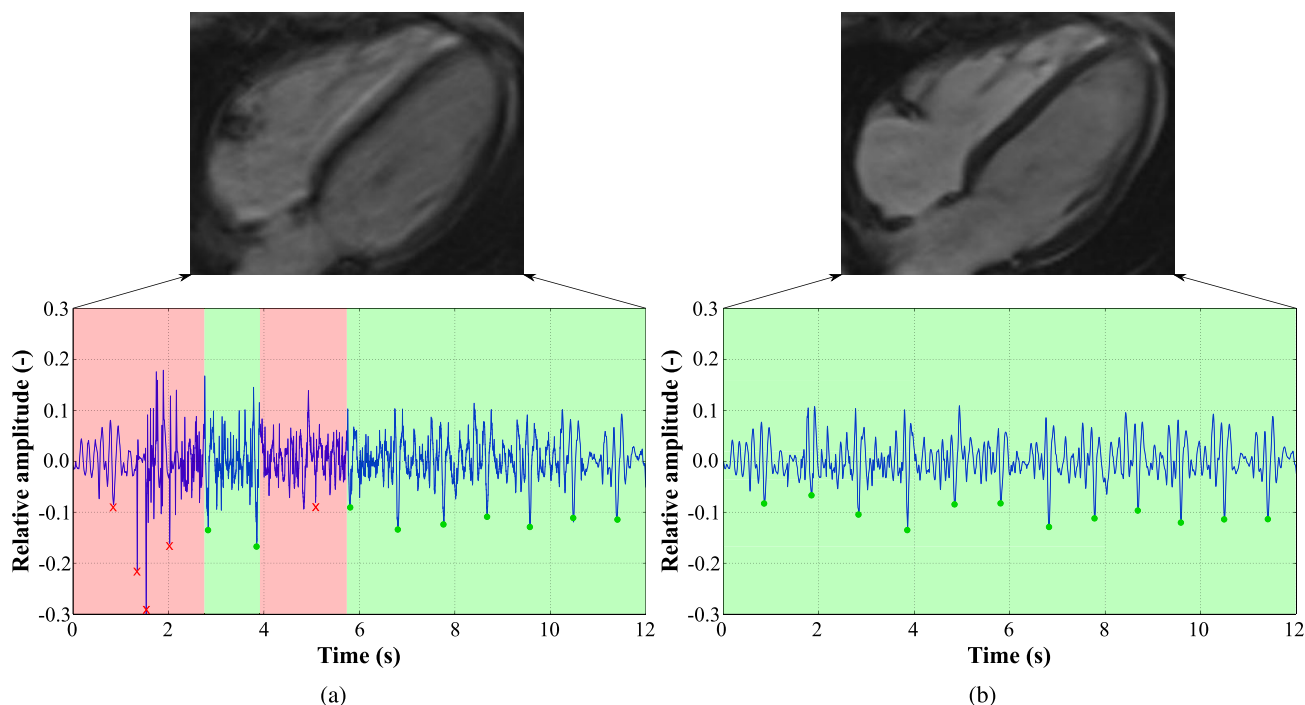
**FIGURE 25.** Results of adaptive filtering using the LMS algorithm from triggering perspective: (a) BCG signal after adaptive filtering; (b) BCG signal after adaptive filtering followed a by low-pass IIR filter of Butterworth approximation with a cut-off frequency of 15 Hz.
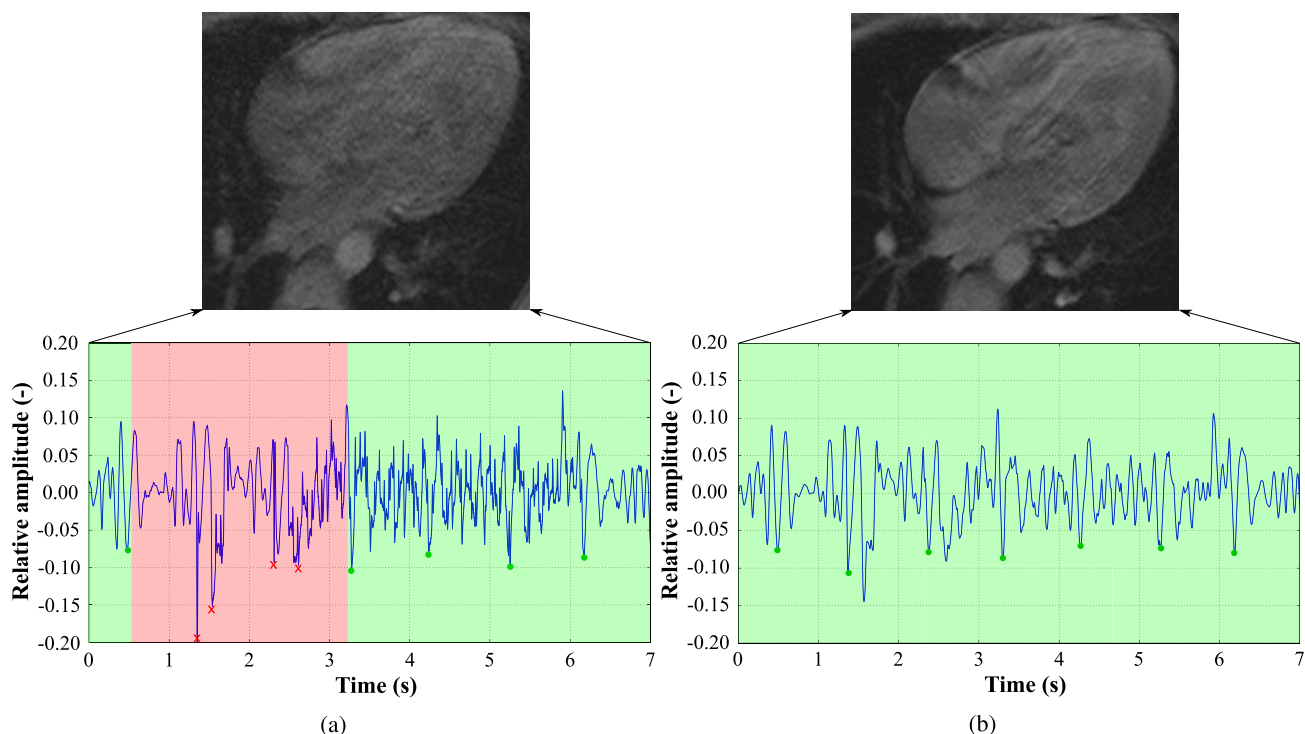


**FIGURE 26.** Results of adaptive filtering using the LMS algorithm from triggering perspective: (a) BCG signal after adaptive filtering; (b) BCG signal after adaptive filtering followed a by low-pass IIR filter of Butterworth approximation with a cut-off frequency of 15 Hz.

Another direction of the research will be verification of functionality for imaging the heart at ultrahigh magnetic fields (7.0 T). According to study [33], triggering within 7.0 T

using acoustic signals achieves better results than ECG-based systems. The study by Krug *et al.* [8] and Snyder *et al.* [9] has shown that triggering with ECG signal is unsuitable for

intensities higher than 3T. The study by Frauenrath *et al.* [10] reports that the error rate while determining the ECG heart rate is up to 30%. It can be assumed that the BCG pneumatic system implemented at 7.0 T will achieve comparable results as in this study, but this needs to be verified experimentally.

The pre-clinical study conducted in ten subjects confirmed the functionality of the proposed system by both subjective and objective evaluation methods. The results of peak classification are consistent with Bland-Altman analysis with ACC values ranging from 92.2% to 99.8% and F1 score ranging from 95.9% to 99.8% with the results of more than half of the subjects being above 95%. The results are comparable to study [36], where the authors tested a low-cost system for seismocardiography-based cardiac triggering on 18 subjects. In this study, the sensor was fastened in the chest area by an elastic band. The new sensor concept without the need to fix it on the patient's body brings many advantages:

- Study [36] was faced with problems of fixing the sensor in female subjects. The new concept shows identical results for both female and male subjects. There are no problems with fixing the sensor to the patient's body.
- Thanks to the concept of the measuring and reference pneumatic system within a single pad that was presented, technical, mechanical and acoustic MRI artifacts can be eliminated very effectively using adaptive filtering. The results presented unequivocally confirm that signal processing methods play a key role in terms of triggering efficiency. The study presents the importance of adaptive filtering as well as preprocessing by means of IIR filter. This area will be the subject of further research.
- Due to the design of the pneumatic sensor, the waveforms of BCG signals have different waveforms compared to the waveforms of SCG signals, where the membrane was formed by the human body [36]. It can be stated that, from the perspective of triggering using J-J, or A0-A0, interval, the new concept is more advantageous, see Fig. 27. An important conclusion of the pre-clinical study is that the waveforms of BCG differ slightly from subject to subject. In study [36], the waveforms varied significantly for different subjects, which greatly increased the demands on the A0-A0 interval detector and could often lead to error.
- Based on the pre-clinical study conducted, it can be hypothesized that the proposed system has the ambition to shorten the examination time and also to increase patient comfort. Nevertheless, this hypothesis will have to be verified by a larger clinical study that will cover the full spectrum of patients.
- Based on the pre-clinical study conducted, it can be hypothesized that the proposed system has the ambition for the application of the so-called double continuous triggering by means of cardiac and respiratory activity. The possibilities of using the pneumatic system for respiratory triggering were not the subject of this study. However, data analysis revealed that the data contained
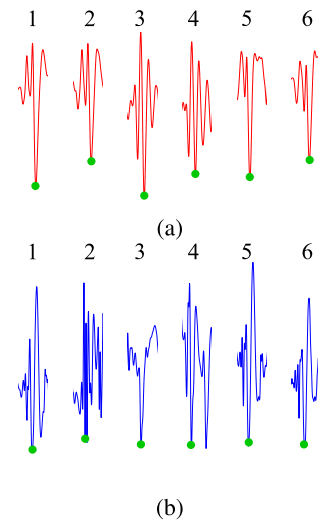


**FIGURE 27.** Comparison of the waveforms of the signals (a) sensor in the bed embodiment - BCG; (b) sensor in the funnel embodiment - SCG.
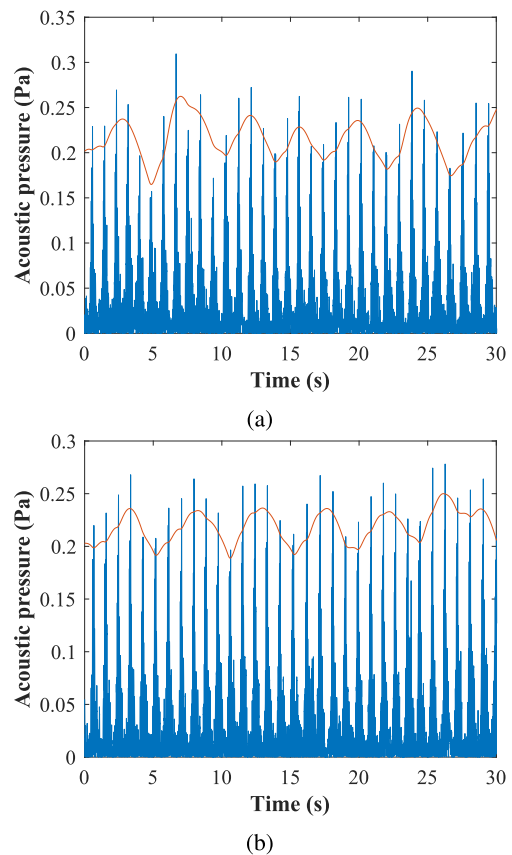


**FIGURE 28.** A sample of respiratory activity detection.

a modulated signal that represents respiratory activities, see Fig. 28. The team of authors has experience with respiratory triggering [73]. Conducting a pre-clinical study that focuses on respiratory triggering will be the subject of further research.

At the same time, it is also necessary to realize that the patient's respiratory cycle information is usually most strongly transmitted by the change of the centre of gravity.

Thus, in the case of the sensor being tested, a hybrid system, which can continuously sense cardiac and respiratory activity without the need to fix the sensor to the patient, can be taken into consideration. At present, there is no system in clinical practice that allows the so-called "double" triggering. It can be stated that such an approach is a major challenge of the current clinical practice. Such an approach would bring a number of advantages to physicians:

- The standard examination time for one CMRI sequence requires respiratory cooperation for a period from 5 to 20 seconds, depending on the rate of cardiac action. Depending on the size of the heart, the standard examination consists of 40 to 60 inhalations, which means the total length of the examination ranges from 30 to 50 minutes when administering a contrast medium, depending on the heart size and respiratory cooperation. The concept proposed may lead to a shorter overall examination time, even if individual sequences become longer due to respiratory triggering. We eliminate repetition of respiratorily blurred sequences, i.e. the diagnostic benefit is enhanced by acquiring images without respiratory artifacts.

- Patients undergoing cardiac examination are usually limited by reduced cardiac function, they have a problem taking repeated breaths for a period from 12 to 15 seconds in a row, and, due to their reduced performance, these breaths are associated with motion artifacts from the respiratory activity. The respiratory triggering itself will extend the individual sequences, but, overall, we expect sharp images that will not require repetition of blurred images, thus shortening the examination time. The benefit is the possibility of examining a non-cooperating patient who can breathe freely during the examination, which brings higher comfort and, above all, the feasibility of the examination.

Based on this pilot pre-clinical study, the sensor designed has the potential to become a universal sensor since its functionality is not affected by the patient's physical parameters, as for example in study [36]. It will allow to examining non-cooperating patients, whether for limiting cardiac function or respiratory problems, and it will also allow examining patients in a coma or small children. Part of the MR examination of the heart is terminated prematurely due to the inability to continue caused by the patient's intolerance - they are unable to continue to cooperate successfully; the use of a combined sensor allows a smoother and successful test run with a valid result - there will be no need for repeated attempts to perform a successful examination.

## V. CONCLUSION

This pilot study compared the novel monitoring system for cardiac triggering using BCG with conventional systems based on ECG and PPG. The proposed pad system is advantageous for the clinical use since it is not necessary to fix it on the patient's body, which can reduce the length of preparation as well as the procedure itself and thus increase patient's comfort and decrease the examination costs. The study was conducted on 10 subjects at the Siemens Prisma 3T MRI Scanner and compared with conventional monitoring methods (ECG and PPG). For all subjects, the total accuracy reached 96.31% and F1 score reached 98.18%.

Objective methods of image quality evaluation using BRISQUE, NIQE, PIQE methods were also used for the evaluation. These methods also confirmed the functionality of the system tested compared to ECG and PPG. However, it should be noted that these methods are not able to capture diagnostically significant parts, as they only compare the image quality and do not take into account the clinical information. For these reasons, the study also includes a blind subjective test (by 10 experts). This test also confirmed the functionality of the sensor tested. The BCG system outperformed the conventional PPG-based system and was comparable to the ECG-based one.

In the concept of the pneumatic sensor presented, a gaseous medium is used. The use of a liquid medium will be the subject of further research. This approach should unequivocally lead to an increase in speed, or the system response, which, in the opinion of the team of authors, could lead to better results since the propagation delay of the BCG signal will be minimized. Furthermore, it can be assumed that the sensitivity of the sensor will increase. However, these hypotheses need to be verified experimentally in future clinical studies.

## ETHICS STATEMENT

*Ref. No.:* EKV-2018-010
*Project Title:* MR imaging sequences and protocols optimization aiming to application of new coil and pulse sequences
*Proposal:* 0319/2018
*Investigator:* Ing. Lubomir Vojtisek, Ph.D.
*Organisational Unit:* CEITEC

The Research Ethics Committee of Masaryk University has reviewed the application to conduct the research project as specified above and on 8 June 2018 the Committel has approved this project to be conducted. The Committee expects to be informed about any revision in the research protocols and/or informed consent form and ask to be provided a copy of the final report.

## REFERENCES

[1] T. Niendorf, D. K. Sodickson, G. A. Krombach, and J. Schulz-Menger, "Toward cardiovascular MRI at 7 T: Clinical needs, technical solutions and research promises," *Eur. Radiol.*, vol. 20, no. 12, pp. 2806–2816, Dec. 2010. [Online]. Available: http://link.springer.com/10.1007/s00330-010-1902-8

[2] A. Varghese and D. J. Pennell, *Cardiovascular Magnetic Resonance Made Easy*. Amsterdam, The Netherlands: Elsevier, 2007.

[3] *MRI Protocols, MRI Planning, MRI Techniques and Anatomy*. Accessed: Jan. 1, 2020. [Online]. Available: https://mrimaster.com/

[4] M. S. Nacif, A. Zavodni, N. Kawel, E.-Y. Choi, J. A. C. Lima, and D. A. Bluemke, "Cardiac magnetic resonance imaging and its electrocardiographs (ECG): Tips and tricks," *Int. J. Cardiovascular Imag.*, vol. 28, no. 6, pp. 1465–1475, Aug. 2012. [Online]. Available: http://link.springer.com/10.1007/s10554-011-9957-4

[5] H. Kugel, C. Bremer, M. Püschel, R. Fischbach, H. Lenzen, B. Tombach, H. Van Aken, and W. Heindel, "Hazardous situation in the MR bore: Induction in ECG leads causes fire," *Eur. Radiol.*, vol. 13, no. 4, pp. 690–694, Apr. 2003.

[6] S. Lange and Q. N. Nguyen, "Cables and electrodes can burn patients during MRI," *Nursing*, vol. 36, no. 11, p. 18, Nov. 2006.

[7] G. M. Pohost and K. S. Nayak, *Handbook of Cardiovascular Magnetic Resonance Imaging*. Boca Raton, FL, USA: CRC Press, 2006.

[8] J. Krug, G. Rose, D. Stucht, G. Clifford, and J. Oster, "Limitations of VCG based gating methods in ultra high field cardiac MRI," *J. Cardiovascular Magn. Reson.*, vol. 15, no. S1, p. W19, Jan. 2013. [Online]. Available: https://jcmr-online.biomedcentral.com/articles/10.1186/1532-429X-15-S1-W19

[9] C. Snyder, L. Delabarre, G. Metzger, P.-F. Van De Moortele, C. Akgun, K. Ugurbil, and J. Vaughan, "Initial results of cardiac imaging at 7 tesla," *Magn. Reson. Med.*, vol. 61, no. 3, pp. 517–524, Mar. 2009, doi: 10.1002/mrm.21895.

[10] T. Frauenrath, F. Hezel, W. Renz, T. D. G. D'orth, M. Dieringer, F. von Knobelsdorff-Brenkenhoff, M. Prothmann, J. Schulz-Menger, and T. Niendorf, "Acoustic cardiac triggering: A practical solution for synchronization and gating of cardiovascular magnetic resonance at 7 tesla," *J. Cardiovascular Magn. Reson.*, vol. 12, no. 1, p. 67, Dec. 2010. [Online]. Available: https://jcmr-online.biomedcentral.com/articles/10.1186/1532-429X-12-67

[11] D. Abi-Abdallah, V. Robin, A. Drochon, and O. Fokapu, "Alterations in human ECG due to the MagnetoHydroDynamic effect: A method for accurate R peak detection in the presence of high MHD artifacts," in *Proc. 29th Annu. Int. Conf. IEEE Eng. Med. Biol. Soc.*, Lyon, France, Aug. 2007, pp. 1842–1845. [Online]. Available: http://ieeexplore.ieee.org/document/4352673/

[12] M. Schmidt, J. W. Krug, A. Gierstorfer, and G. Rose, "A real-time QRS detector based on higher-order statistics for ECG gated cardiac MRI," in *Proc. IEEE Comput. Cardiol.*, Sep. 2014, pp. 733–736.

[13] D. Abi-Abdallah, A. Drochon, V. Robin, and O. Fokapu, "Cardiac and respiratory MRI gating using combined wavelet sub–band decomposition and adaptive filtering," *Ann. Biomed. Eng.*, vol. 35, no. 5, pp. 733–743, Apr. 2007. [Online]. Available: http://link.springer.com/10.1007/s10439-007-9285-y

[14] E. D. Allen and J. H. Burdette, *Questions and Answers in MRI*, vol. 7, no. 14, 2nd ed. St. Louis, MO, USA: Univ. of Maryland, 2001, p. 14.

[15] N. Spicher, M. Kukuk, S. Maderwald, and M. E. Ladd, "Initial evaluation of prospective cardiac triggering using photoplethysmography signals recorded with a video camera compared to pulse oximetry and electrocardiography at 7t MRI," *Biomed. Eng. OnLine*, vol. 15, no. 1, p. 126, Dec. 2016. [Online]. Available: http://biomedical-engineering-online.biomedcentral.com/articles/10.1186/s12938-016-0245-3

[16] A. C. Larson, R. D. White, G. Laub, E. R. Mcveigh, D. Li, and O. P. Simonetti, "Self-gated cardiac cine MRI," *Magn. Reson. Med.*, vol. 51, no. 1, pp. 93–102, Jan. 2004, doi: 10.1002/mrm.10664.

[17] A. C. Larson, P. Kellman, A. Arai, G. A. Hirsch, E. Mcveigh, D. Li, and O. P. Simonetti, "Preliminary investigation of respiratory self-gating for free-breathing segmented cine MRI," *Magn. Reson. Med.*, vol. 53, no. 1, pp. 159–168, Jan. 2005, doi: 10.1002/mrm.20331.

[18] B. Hiba, N. Richard, M. Janier, and P. Croisille, "Cardiac and respiratory double self-gated cine MRI in the mouse at 7 T," *Magn. Reson. Med.*, vol. 55, no. 3, pp. 506–513, Mar. 2006, doi: 10.1002/mrm.20815.

[19] M. E. Crowe, A. C. Larson, Q. Zhang, J. Carr, R. D. White, D. Li, and O. P. Simonetti, "Automated rectilinear self-gated cardiac cine imaging," *Magn. Reson. Med.*, vol. 52, no. 4, pp. 782–788, Oct. 2004, doi: 10.1002/mrm.20212.

[20] M. Becker, T. Frauenrath, F. Hezel, G. A. Krombach, U. Kremer, B. Koppers, C. Butenweg, A. Goemmel, J. F. Utting, J. Schulz-Menger, and T. Niendorf, "Comparison of left ventricular function assessment using phonocardiogram- and electrocardiogram-triggered 2D SSFP CINE MR imaging at 1.5 T and 3.0 T," *Eur. Radiol.*, vol. 20, no. 6, pp. 1344–1355, Jun. 2010. [Online]. Available: http://link.springer.com/10.1007/s00330-009-1676-z

[21] F. Kording, J. Yamamura, G. Lund, F. Ueberle, C. Jung, G. Adam, and B. P. Schoennagel, "Doppler ultrasound triggering for cardiovascular MRI at 3t in a healthy volunteer study," *Magn. Reson. Med. Sci.*, vol. 16, no. 2, pp. 98–108, 2017. [Online]. Available: https://www.jstage.jst.go.jp/article/mrms/16/2/16_mp.2015-0104/_article

[22] J. M. Rubin, J. Brian Fowlkes, M. R. Prince, R. T. Rhee, and T. L. Chenevert, "Doppler US gating of cardiac MR imaging," *Acad. Radiol.*, vol. 7, no. 12, pp. 1116–1122, Dec. 2000. [Online]. Available: https://linkinghub.elsevier.com/retrieve/pii/S1076633200800653

[23] F. Kording, B. Schoennagel, G. Lund, F. Ueberle, C. Jung, G. Adam, and J. Yamamura, "Doppler ultrasound compared with electrocardiogram and pulse oximetry cardiac triggering: A pilot study: Alternative trigger technique for cardiac MRI using DUS," *Magn. Reson. Med.*, vol. 74, no. 5, pp. 1257–1265, Nov. 2015, doi: 10.1002/mrm.25502.

[24] D. A. Feinberg, D. Giese, D. A. Bongers, S. Ramanna, M. Zaitsev, M. Markl, and M. Günther, "Hybrid ultrasound MRI for improved cardiac imaging and real-time respiration control," *Magn. Reson. Med.*, vol. 63, no. 2, pp. 290–296, Feb. 2010, doi: 10.1002/mrm.22250.

[25] A. C. Brau, C. T. Wheeler, L. W. Hedlund, and G. A. Johnson, "Fiber-optic stethoscope: A cardiac monitoring and gating system for magnetic resonance microscopy," *Magn. Reson. Med.*, vol. 47, no. 2, pp. 314–321, Feb. 2002, doi: 10.1002/mrm.10049.

[26] A. Rengle, L. Baboi, H. Saint-Jalmes, R. Sablong, and O. Beuf, "Optical cardiac and respiratory device for synchronized MRI on small animal," in *Proc. 29th Annu. Int. Conf. IEEE Eng. Med. Biol. Soc.*, Lyon, France, Aug. 2007, pp. 2046–2049. [Online]. Available: http://ieeexplore.ieee.org/document/4352722/

[27] J. Nedoma, M. Fajkus, M. Novak, N. Strbikova, V. Vasinek, H. Nazeran, J. Vanus, F. Perecar, and R. Martinek, "Validation of a novel fiber-optic sensor system for monitoring cardiorespiratory activities during MRI examinations," *Adv. Electr. Electron. Eng.*, vol. 15, no. 3, pp. 536–543, Oct. 2017. [Online]. Available: http://advances.utc.sk/index.php/AEEE/article/view/2194

[28] Ł. Dziuda, M. Krej, and F. W. Skibniewski, "Fiber Bragg grating strain sensor incorporated to monitor patient vital signs during MRI," *IEEE Sensors J.*, vol. 13, no. 12, pp. 4986–4991, Dec. 2013. . [Online]. Available: http://ieeexplore.ieee.org/document/6585757/

[29] Ł. Dziuda, F. W. Skibniewski, M. Krej, and P. M. Baran, "Fiber Bragg grating-based sensor for monitoring respiration and heart activity during magnetic resonance imaging examinations," *J. Biomed. Opt*, vol. 18, no. 5, May 2013, Art. no. 057006. [Online]. Available: http://biomedicaloptics.spiedigitallibrary.org/article.aspx?doi=10.1117/1.JBO.18.5.057006

[30] J. Nedoma, S. Kepak, M. Fajkus, J. Cubik, P. Siska, R. Martinek, and P. Krupa, "Magnetic resonance imaging compatible non–invasive fibre–optic sensors based on the Bragg gratings and interferometers in the application of monitoring heart and respiration rate of the human body: A comparative study," *Sensors*, vol. 18, no. 11, p. 3713, Oct. 2018. [Online]. Available: http://www.mdpi.com/1424-8220/18/11/3713

[31] Ł. Dziuda and F. W. Skibniewski, "A new approach to ballistocardiographic measurements using fibre Bragg grating-based sensors," *Biocybernetics Biomed. Eng.*, vol. 34, no. 2, pp. 101–116, 2014. [Online]. Available: https://linkinghub.elsevier.com/retrieve/pii/S0208521614000187

[32] S. Maderwald, S. Orzada, Z. Lin, L. C. Schafer, A. K. Bitz, O. Kraff, and K. Nassenstein, "7 tesla cardiac imaging with a phonocardiogram trigger device," in *Proc. Int. Soc. Mag. Reson. Med.*, vol. 19, 2011, p. 1322.

[33] T. Frauenrath, S. Kozerke, P. Boesiger, and T. Niendorf, "Cardiac gating free of interference with electro-magnetic fields at 1.5 T, 3.0 T and 7.0 T," in *Proc. Annu. Meeting Int. Soc. Magn. Res. Med.*, 2008, p. 207.

[34] K. Nassenstein, S. Orzada, L. Haering, A. Czylwik, M. Zenge, H. Eberle, T. Schlosser, O. Bruder, E. Müller, M. E. Ladd, and S. Maderwald, "Cardiac MRI: evaluation of phonocardiogram-gated cine imaging for the assessment of global und regional left ventricular function in clinical routine," *Eur. Radiol.*, vol. 22, no. 3, pp. 559–568, Mar. 2012. [Online]. Available: http://link.springer.com/10.1007/s00330-011-2279-z

[35] T. Frauenrath, T. Niendorf, and M. Kob, "Acoustic method for synchronization of magnetic resonance imaging (MRI)," *Acta Acustica United Acustica*, vol. 94, no. 1, pp. 148–155, Jan. 2008. [Online]. Available: http://openurl.ingenta.com/content/xref?genre=article&issn=1610-1928&volume=94&issue=1&spage=148

[36] R. Martinek, J. Brablik, J. Kolarik, M. Ladrova, J. Nedoma, R. Jaros, L. Soustek, R. Kahankova, M. Fajkus, L. Vojtisek, P. Hanzlikova, and P. Krupa, "A low–cost system for seismocardiography–based cardiac triggering: A practical solution for cardiovascular magnetic resonance imaging at 3 tesla," *IEEE Access*, vol. 7, pp. 118608–118629, 2019. [Online]. Available: https://ieeexplore.ieee.org/document/8805311/

[37] A. Dinh, Y. Choi, and S.-B. Ko, "A heart rate sensor based on seismocardiography for vital sign monitoring systems," in *Proc. IEEE 24th Can. Conf. Elect. Comput. Eng. (CCECE)*, Niagara Falls, ON, Canada, May 2011, pp. 665–668. [Online]. Available: http://ieeexplore.ieee.org/document/6030536/

[38] M. Jerosch-Herold, J. Zanetti, H. Merkle, L. Poliac, H. Huang, A. Mansoor, F. Zhao, and N. Wilke, "The seismocardiogram as magnetic-field-compatible alternative to the electrocardiogram for cardiac stress monitoring," *Int. J. Cardiac Imag.*, vol. 15, no. 6, pp. 523–531, 1999. [Online]. Available: http://link.springer.com/10.1023/A:1006364518204

[39] M. Fajkus, J. Nedoma, R. Martinek, V. Vasinek, H. Nazeran, and P. Siska, "A non–invasive multichannel hybrid fiber–optic sensor system for vital sign monitoring," *Sensors*, vol. 17, no. 12, p. 111, Jan. 2017. [Online]. Available: http://www.mdpi.com/1424-8220/17/1/111

[40] M. Krej, Ł. Dziuda, and F. W. Skibniewski, "A method of detecting heartbeat locations in the ballistocardiographic signal from the fiber–optic vital signs sensor," *IEEE J. Biomed. Health Inform.*, vol. 19, no. 4, pp. 1443–1450, Jul. 2015. [Online]. Available: http://ieeexplore.ieee.org/document/7018891/

[41] O. T. Inan, P.-F. Migeotte, K.-S. Park, M. Etemadi, K. Tavakolian, R. Casanella, J. Zanetti, J. Tank, I. Funtova, G. K. Prisk, and M. Di Rienzo, "Ballistocardiography and seismocardiography: A review of recent advances," *IEEE J. Biomed. Health Inform.*, vol. 19, no. 4, pp. 1414–1427, Jul. 2015. [Online]. Available: http://ieeexplore.ieee.org/document/6916998/

[42] M. Haescher, D. J. C. Matthies, J. Trimpop, and B. Urban, "A study on measuring heart- and respiration-rate via wrist-worn accelerometer-based seismocardiography (SCG) in comparison to commonly applied technologies," in *Proc. 2nd ACM Int. Workshop Sensor-Based Activity Recognit. Interact. (WOAR)*, Rostock, Germany, 2015, pp. 1–6. [Online]. Available: http://dl.acm.org/citation.cfm?doid=2790044.2790054

[43] O. Postolache, P. Girão, and G. Postolache, "Seismocardiogram and ballistocardiogram sensing," in *Advanced Instrument Engineering: Measurement, Calibration, and Design*. Harrisburg, PA, USA: IGI Global, 2013, pp. 223–246.

[44] R. Jaros, R. Martinek, R. Kahankova, and J. Koziorek, "Novel hybrid extraction systems for fetal heart rate variability monitoring based on non–invasive fetal electrocardiogram," *IEEE Access*, vol. 7, pp. 131758–131784, 2019. [Online]. Available: https://ieeexplore.ieee.org/document/8790705/

[45] V. Wu, I. M. Barbash, K. Ratnayaka, C. E. Saikus, M. Sonmez, O. Kocaturk, R. J. Lederman, and A. Z. Faranesh, "Adaptive noise cancellation to suppress electrocardiography artifacts during real-time interventional MRI," *J. Magn. Reson. Imag.*, vol. 33, no. 5, pp. 1184–1193, May 2011, doi: 10.1002/jmri.22530.

[46] G. Sun, M. Li, B. W. Rudd, T. C. Lim, J. Osterhage, E. M. Fugate, and J.-H. Lee, "Adaptive speech enhancement using directional microphone in a 4-T MRI scanner," *Magn. Reson. Mater. Phys., Biol. Med.*, vol. 28, no. 5, pp. 473–484, Oct. 2015. [Online]. Available: http://link.springer.com/10.1007/s10334-015-0485-4

[47] A. Mittal, A. K. Moorthy, and A. C. Bovik, "No–reference image quality assessment in the spatial domain," *IEEE Trans. Image Process.*, vol. 21, no. 12, pp. 4695–4708, Dec. 2012. [Online]. Available: http://ieeexplore.ieee.org/document/6272356/

[48] A. Mittal, A. K. Moorthy, and A. C. Bovik, "Referenceless image spatial quality evaluation engine," in *Proc. 45th Asilomar Conf. Signals, Syst. Comput.*, vol. 38, 2011, pp. 53–54.

[49] A. Mittal, R. Soundararajan, and A. C. Bovik, "Making a 'completely blind' image quality analyzer," *IEEE Signal Process. Lett.*, vol. 20, no. 3, pp. 209–212, Mar. 2013. [Online]. Available: http://ieeexplore.ieee.org/document/6353522/

[50] Venkatanath N, Praneeth D, Maruthi Chandrasekhar Bh, S. S. Channappayya, and S. S. Medasani, "Blind image quality evaluation using perception based features," in *Proc. 21st IEEE Nat. Conf. Commun. (NCC)*, Mumbai, India, Feb./Mar. 2015, pp. 1–6. [Online]. Available: http://ieeexplore.ieee.org/document/7084843/

[51] H. R. Sheikh. (2005). *LIVE Image Quality Assessment Database Release 2*. [Online]. Available: http://live.ece.utexas.edu/research/quality

[52] J. M. Bland and D. G. Altman, "Measuring agreement in method comparison studies," *Stat. Methods Med. Res.*, vol. 8, no. 2, pp. 135–160, Apr. 1999. [Online]. Available: http://journals.sagepub.com/doi/10.1177/096228029900800204

[53] R. Martinek, R. Kahankova, H. Nazeran, J. Konecny, J. Jezewski, P. Janku, P. Bilik, J. Zidek, J. Nedoma, and M. Fajkus, "Non–invasive fetal monitoring: A maternal surface ECG electrode placement–based novel approach for optimization of adaptive filter control parameters using the LMS and RLS algorithms," *Sensors*, vol. 17, no. 5, p. 1154, May 2017. [Online]. Available: http://www.mdpi.com/1424-8220/17/5/1154

[54] M. Maniruzzaman, K. M. S. Billah, U. Biswas, and B. Gain, "Least-mean-square algorithm based adaptive filters for removing power line interference from ECG signal," in *Proc. IEEE Int. Conf. Inform., Electron. Vis. (ICIEV)*. Dhaka, Bangladesh, May 2012, pp. 737–740. [Online]. Available: http://ieeexplore.ieee.org/document/6317472/

[55] R. Kahankova, R. Martinek, R. Jaros, K. Behbehani, A. Matonia, M. Jezewski, and J. A. Behar, "A review of signal processing techniques for non-invasive fetal electrocardiography," *IEEE Rev. Biomed. Eng.*, to be published. [Online]. Available: https://ieeexplore.ieee.org/document/8820039/

[56] U. Biswas, A. Das, S. Debnath, and I. Oishee, "ECG signal denoising by using least-mean-square and normalised-least-mean-square algorithm based adaptive filter," in *Proc. IEEE Int. Conf. Inform., Electron. Vis. (ICIEV)*, Dhaka, Bangladesh, May 2014, pp. 1–6. [Online]. Available: http://ieeexplore.ieee.org/document/6850857/

[57] M. Z. Ur Rahman, R. A. Shaik, and D. V. R. K. Reddy, "Adaptive noise removal in the ECG using the block LMS algorithm," in *Proc. IEEE 2nd Int. Conf. Adapt. Sci. Technol. (ICAST)*, Accra, Ghana, Dec. 2009, pp. 380–383. [Online]. Available: http://ieeexplore.ieee.org/document/5409698/

[58] A. A. Khalaf, M. M. Ibrahim, H. F. A. Hamed, and M. A. Abdelghany, "ECG noise canceller: Studying and performance improvement under different algorithms," in *Proc. 16th Int. Conf. Aerosp. Sci. Aviation Technol.*, 2015.

[59] R. Martinek, J. Zidek, P. Bilik, J. Manas, J. Koziorek, Z. Teng, and H. Wen, "The use of LMS and rls adaptive algorithms for an adaptive control method of active power filter," *Energy Power Eng.*, vol. 5, no. 4, pp. 1126–1133, 2013. [Online]. Available: http://www.scirp.org/journal/PaperDownload.aspx?DOI=10.4236/epe.2013.54B215

[60] R. Kahankova, R. Martinek, and P. Bilik, "Fetal ECG extraction from abdominal ECG using RLS based adaptive algorithms," in *Proc. IEEE 18th Int. Carpathian Control Conf. (ICCC)*, Sinaia, Romania, May 2017, pp. 337–342. [Online]. Available: http://ieeexplore.ieee.org/document/7970422/

[61] A. C. Mugdha, F. S. Rawnaque, and M. U. Ahmed, "A study of recursive least squares (RLS) adaptive filter algorithm in noise removal from ECG signals," in *Proc. IEEE Int. Conf. Inform. Electron. Vis. (ICIEV)*, Fukuoka, Japan, Jun. 2015, pp. 1–6. [Online]. Available: http://ieeexplore.ieee.org/document/7333998/

[62] R. Vullings, B. de Vries, and J. W. M. Bergmans, "An adaptive Kalman filter for ECG signal enhancement," *IEEE Trans. Biomed. Eng.*, vol. 58, no. 4, pp. 1094–1103, Apr. 2011. [Online]. Available: http://ieeexplore.ieee.org/document/5667049/

[63] M. Bin Ibne Reaz and S. Wei, "Adaptive linear neural network filter for fetal ECG extraction," in *Proc. IEEE Int. Conf. Intell. Sens. Inf. Process.*, Chennai, India, Jan. 2004, pp. 321–324. [Online]. Available: http://ieeexplore.ieee.org/document/1287675/

[64] R. Martinek and J. Žídek, "Refining the diagnostic quality of the abdominal fetal electrocardiogram using the techniques of artificial intelligence," Przegląd Elektrotechniczny, Tech. Rep. R.88 NR 12b/2012, 2012.

[65] J.-S. Jang, "ANFIS: Adaptive-network-based fuzzy inference system," *IEEE Trans. Syst., Man, Cybern., Syst.*, vol. 23, no. 3, pp. 665–685, Jun. 1993. [Online]. Available: http://ieeexplore.ieee.org/document/256541/

[66] B. Widrow and M. A. Lehr, "30 years of adaptive neural networks: Perceptron, madaline, and backpropagation," *Proc. IEEE*, vol. 78, no. 9, pp. 1415–1442, Sep. 1990.

[67] A. Hyvärinen and E. Oja, "Independent component analysis: Algorithms and applications," *Neural Netw.*, vol. 13, nos. 4–5, pp. 411–430, Jun. 2000. [Online]. Available: https://linkinghub.elsevier.com/retrieve/pii/S0893608000000265

[68] R. Sameni, C. Jutten, and M. B. Shamsollahi, "What ICA provides for ECG processing: Application to noninvasive fetal ECG extraction," in *Proc. IEEE Int. Symp. Signal Process. Inf. Technol.*, Vancouver, BC, Canada, Aug. 2006, pp. 656–661. [Online]. Available: https://ieeexplore.ieee.org/document/4042324/

[69] D. Luo, "Research and application of fetal electrocardiogram blind signal separation technology," *Res. J. Appl. Sci. Eng. Technol.*, vol. 4, no. 14, pp. 2231–2235, 2012.

[70] R. Jaros, R. Martinek, and R. Kahankova, "Non-adaptive methods for fetal ECG signal processing: A review and appraisal," *Sensors*, vol. 18, no. 11, p. 3648, Oct. 2018. [Online]. Available: http://www.mdpi.com/1424-8220/18/11/3648

[71] R. Martinek, R. Kahankova, J. Nedoma, M. Fajkus, and K. Cholevova, "Fetal ECG preprocessing using wavelet transform," in *Proc. ACM 10th Int. Conf. Comput. Modeling Simulation*, 2018, pp. 39–43.

[72] A. Agostinelli, M. Grillo, A. Biagini, C. Giuliani, L. Burattini, S. Fioretti, F. Di Nardo, S. R. Giannubilo, A. Ciavattini, and L. Burattini, "Non-invasive fetal electrocardiography: An overview of the signal electro-physiological meaning, recording procedures, and processing techniques: Noninvasive fetal electrocardiography," *Ann. Noninvasive Electrocardiol.*, vol. 20, no. 4, pp. 303–313, Jul. 2015, doi: 10.1111/anec.12259.

[73] M. Fajkus, J. Nedoma, R. Martinek, J. Brablik, J. Vanus, M. Novak, S. Zabka, V. Vasinek, P. Hanzlikova, and L. Vojtisek, "MR fully compatible and safe FBG breathing sensor: A practical solution for respiratory triggering," *IEEE Access*, vol. 7, pp. 123013–123025, 2019. [Online]. Available: https://ieeexplore.ieee.org/document/8813026/

**RADEK MARTINEK** was born in Czech Republic, in 1984. He received the master's degree in information and communication technology from the VŠB–Technical University of Ostrava, in 2009. Since 2012, he has been a Research Fellow. In 2014, he successfully defended his dissertation thesis titled The Use of Complex Adaptive Methods of Signal Processing for Refining the Diagnostic Quality of the Abdominal Fetal Electrocardiogram. He has become an Associate Professor in technical cybernetics, in 2017, after defending the habilitation thesis titled Design and Optimization of Adaptive Systems for Applications of Technical Cybernetics and Biomedical Engineering Based on Virtual Instrumentation. He has also been an Associate Professor with the VSB–Technical University of Ostrava, since 2017. His current research interests include digital signal processing (linear and adaptive filtering, soft computing - artificial intelligence and adaptive fuzzy systems, non-adaptive methods, biological signal processing, digital processing of speech signals), wireless communications (software-defined radio), power quality improvement. He has more than 200 journal and conference papers in his research areas.

**JINDRICH BRABLIK** was born in 1991. He graduated from the Faculty of Electrical Engineering and Computer Science, VŠB–Technical University of Ostrava. The field of study was biomedical technician for bachelor studies and information and control systems for master studies. He is currently pursuing the Ph.D. degree in technical cybernetics with the VŠB–Technical University of Ostrava, where he focuses on virtual instrumentation and signal processing of physiological signals.

**JAKUB KOLARIK** was born in Ostrava, Czech Republic, in 1992. He received the bachelor's degree from the Department of Cybernetics and Biomedical Engineering, VŠB–Technical University of Ostrava, in 2014, and the master's degree in control and information systems from the Department of Cybernetics and Biomedical Engineering. He is currently pursuing the Ph.D. degree in technical cybernetics.

**MARTINA LADROVA** was born in Ostrava, Czech Republic, in 1994. She received the master's degree from the Faculty of Electrical Engineering and Computer Science, VŠB–Technical University of Ostrava, in 2018, where she is currently pursuing the Ph.D. degree. Her research interests include digital signal processing and especially biological signal processing.

**JAN NEDOMA** was born in Czech Republic, in 1988. He received the master's degree in information and communication technology from the VŠB–Technical University of Ostrava, in 2014. Since 2014, he has been a Research Fellow. In 2017, he successfully defended his dissertation thesis and works as an Assistant Professor at the VŠB–Technical University of Ostrava. His current research interests include fiber-optic sensors in traffic, civil engineering, and biomedical applications. He has more than 125 journal and conference papers (Author H-Index: Nine without self-citations) in his research areas and six valid patents.

**RADANA KAHANKOVA** was born in Opava, Czech Republic, in 1991. She received the bachelor's degree from the Department of Cybernetics and Biomedical Engineering, VŠB–Technical University of Ostrava, in 2014, and the master's degree in biomedical engineering from the Department of Cybernetics and Biomedical Engineering. She is currently pursuing the Ph.D. degree in technical cybernetics. Her current research is focused on improving the quality of electronic fetal monitoring.

**RENE JAROS** was born in Ostrava, Czech Republic, in 1992. He graduated from the Faculty of Electrical Engineering and Computer Science, VŠB–Technical University of Ostrava, in 2015. In 2015, he wrote a bachelor thesis, which deals with transformation methods of 12-lead ECG to VCG, and in 2017, he wrote a diploma thesis, which deals with non-adaptive methods of fetal ECG signal processing. In 2019, he successfully defended his dissertation thesis titled Hybrid Methods for Processing of Fetal Electrocardiogram. His current research interest includes improving the quality of electronic fetal monitoring especially on fECG extraction by using hybrid methods.

**LUBOMIR VOJTISEK** received the Ph.D. degree in measurement from the Faculty of Electrical Engineering and Information Technology, Slovak Technical University. He is currently a Researcher and a Technical Specialist Member of the MultiModal and Functional Neuroimaging Research Group. He is also a Postdoctoral Research Fellow.

**PAVLA HANZLIKOVA** is currently with the Clinic of Imaging Methods of Faculty Hospital in Ostrava and deals with interventional neuroradiology, MR spectroscopy, and interventional applications of 3D image.

● ● ●